© 2018. Published by The Company of Biologists Ltd | Development (2018) 145, dev166587. doi:10.1242/dev.166587

RESEARCH ARTICLE

Maternal Ybx1 safeguards zebrafish oocyte maturation and maternal-to-zygotic transition by repressing global translation

Jiawei Sun, Lu Yan, Weimin Shen and Anming Meng*

ABSTRACT

Maternal mRNAs and proteins dictate early embryonic development before zygotic genome activation. In the absence of transcription, elaborate control of maternal mRNA translation is of particular importance for oocyte maturation and early embryogenesis. By analyzing zebrafish *ybx1* mutants with a null allele, we demonstrate an essential role of maternal *ybx1* in repressing global translation in oocytes and embryos. Loss of maternal Ybx1 leads to impaired oocyte maturation and egg activation. Maternal *ybx1* (M*ybx1*) mutant embryos fail to undergo normal cleavage and the maternal-to-zygotic transition (MZT). Morpholino knockdown of *ybx1* also results in MZT loss and epiboly failure, suggesting the postfertilization requirement of Ybx1. In addition, elevated global translation level and the unfolded protein response were found in Ybx1-depleted embryos. Supplementing translational repression by eIF4E inhibition markedly rescues the M*ybx1* phenotype. Mechanistically, Ybx1 in embryos may associate with processing body components and repress translation when tethered to target mRNAs. Collectively, our results identify maternal Ybx1 as a global translational repressor required for oocyte maturation and early embryogenesis.

KEY WORDS: Ybx1, Zebrafish, Oocyte maturation, Embryogenesis, Maternal-to-zygotic transition, Translational repression

INTRODUCTION

Before zygotic genome activation (ZGA), the transcriptionally silent early embryos depend solely on maternally provided materials for the initial stages of development, including fertilization, cleavage and preliminary body plan formation (Abrams and Mullins, 2009). This maternal control of development gradually switches to control by zygotic gene products during the maternal-to-zygotic transition (MZT), which is composed of maternal message decay and ZGA (Lee et al., 2014; Tadros and Lipshitz, 2009; Yartseva and Giraldez, 2015). Similar to pre-MZT embryos, late-stage oocytes that have completed volume expansion and material accumulation are also transcriptionally inactive (Edson et al., 2009). To drive oocyte maturation and early embryogenesis in the absence of transcription, protein synthesis needs to be fine-tuned by dedicated translational regulators targeting subsets of maternal mRNAs (Bazzini et al., 2016; Chen et al., 2013; Giraldez et al., 2006; Miao et al., 2017; Sha et al., 2017; Tadros et al., 2007; Winata et al., 2018). Interestingly, global maternal mRNA translation before the MZT also exhibits unique properties compared with translation in post-MZT embryos and non-embryonic contexts. Translational efficiencies in cleavage- and blastula-stage embryos of zebrafish and *Xenopus* are strongly coupled to poly(A) tail lengths. This coupling is lost in gastrulas, suggesting a developmental switch of translational control (Rabani et al., 2014; Subtelny et al., 2014). Therefore, in addition to sequence-specific RNA-binding proteins, translational regulators with less sequence specificity may also play important roles during early embryonic development.

Y-box binding proteins, including Ybx1, are a group of proteins found in bacteria, plants and animals (Darnbrough and Ford, 1981; Kohno et al., 2003; Sommerville and Ladomery, 1996; Wolffe et al., 1992). They were termed 'Y-box binding' because of early studies that discovered their ability to bind to Y-box DNA elements, although subsequent studies disclosed their relatively low specificity of interaction with DNA and RNA sequences (Didier et al., 1988; Kolluri et al., 1992; Wolffe, 1994; Wolffe et al., 1992). Multiple names, including YB, FRGY and MSY, have been assigned to these proteins. Vertebrate Y-box binding proteins are highly conserved in terms of sequence homology and are enriched in oocytes and spermatocytes (Bouvet and Wolffe, 1994; Darnbrough and Ford, 1981; Sommerville and Ladomery, 1996; Tafuri et al., 1993). They were identified as major components of cytoplasmic messenger ribonucleoproteins (mRNPs), with ubiquitous RNA-binding ability (Bouvet and Wolffe, 1994; Dearsly et al., 1985; Deschamps et al., 1992; Evdokimova et al., 1995; Minich et al., 1993; Murray et al., 1992). In the light of extensive studies over several decades, Y-box proteins have been linked to a wide range of nucleic acid-related processes including translational repression, RNA stabilization and transcriptional regulation (Bouvet and Wolffe, 1994; Evdokimova et al., 2001; Goodarzi et al., 2015; Holm et al., 2002; Meric et al., 1997; Ohga et al., 1998; Svitkin et al., 2009; Tafuri and Wolffe, 1993; Yu et al., 2002). Despite these results, which were mostly from *in vitro* and cell culture systems, the *in vivo* roles of Y-box proteins in developmental and physiological processes remain relatively unclear. *Ybx1* knockout mice exhibit embryonic lethality and neural tube closure defects (Lu et al., 2005; Uchiumi et al., 2006). *Ybx2* knockout leads to female and male infertility in mice, which has been linked to RNA instability in germ cells (Medvedev et al., 2011; Yang et al., 2005, 2007). It remains unclear to what extent the molecular mechanisms discovered *in vitro* contribute to Y-box protein functions *in vivo*.

In zebrafish, Ybx1 protein has been shown to physically associate with the dorsal localization element (DLE) of maternal *sqt/ndr1* mRNA (Kumari et al., 2013), which encodes a Nodal ligand that is critical for mesendodermal induction and patterning following the midblastula transition (see reviews by Schier and Shen, 2000; De Robertis and Kuroda, 2004; Robertson, 2014). Dr Karuna Sampath's group generated two mutant alleles of the zebrafish *ybx1*

Laboratory of Molecular Developmental Biology, State Key Laboratory of Membrane Biology, Tsinghua-Peking Center for Life Sciences, School of Life Sciences, Tsinghua University, Beijing 100084, China.

*Author for correspondence (mengam@mail.tsinghua.edu.cn)

J.S., 0000-0003-4983-624X; L.Y., 0000-0001-8616-3529; A.M., 0000-0001-7228-3431

Received 10 April 2018; Accepted 23 July 2018

Development (2018) 145, dev166587. doi:10.1242/dev.166587

locus: *sa42* and *sg8* (Kumari et al., 2013). Embryos derived from *sa42* homozygous females, referred to as maternal mutants M*ybx1*^{sa42}, developed normally under normal incubation conditions (28.5°C), but, if incubated at 23°C, they formed a larger yolk syncytial layer by blastula stages and failed to initiate gastrulation. In contrast, M*ybx1*^{sg8} mutants at 28.5°C showed abnormal development with aberrant cleavage from the 16-cell stage onward, much earlier than in the stage at which M*ybx1*$_{sa42}$ mutants at 23°C developed their phenotype, and were developmentally arrested. Through extensive studies using M*ybx1*^{sa42} embryos, Kumari et al. propose that maternal Ybx1 is required for *sqt* RNA translocation, processing and translational repression (Kumari et al., 2013). Subsequently, DLEs have also been identified in the 3′UTRs of mRNAs of the Nodal antagonist genes *lefty1* and *lefty2*, and can be bound by Ybx1, which results in translational repression of these zygotic mRNAs in zebrafish embryos (Zaucker et al., 2018). However, it remains unknown whether the function of maternal Ybx1 is restricted to the Nodal pathway components in zebrafish embryos.

In this study, we generated and analyzed zebrafish *ybx1* mutants with a null allele. Although zygotic *ybx1* mutants can develop into adulthood, loss of maternal Ybx1 causes severe defects in egg activation and early embryonic development. Further analyses revealed a crucial role of zebrafish Ybx1 as a general translational repressor in oocytes and early blastulas. Zebrafish Ybx1 exemplifies a regulatory module essential for translational control in early embryos, but dispensable at later stages.

RESULTS

Generation and morphological phenotype of *ybx1* null mutants

To study the *in vivo* role of Ybx1, we employed CRISPR/Cas9 to edit the zebrafish *ybx1* gene. The coding region within the first exon of *ybx1* was targeted and several mutant alleles were generated. We focused on the *ybx1*^{tsu3d5i} allele that harbours a 3-base pair (bp) deletion and a 5-bp insertion (Fig. 1A). This mutation causes a premature stop codon and the truncated Ybx1^{tsu3d5i} protein is predicted to lose the entire cold shock domain (CSD) and C-terminal domain (Fig. 1A). Notably, the CSD is crucial for the nucleic acid-binding ability of Ybx1 (Kohno et al., 2003). Zygotic *ybx1*$^{tsu3d5i/tsu3d5i}$ (Z*ybx1*) mutants, obtained by crossing heterozygotes, showed normal morphology during embryogenesis and could become fertile adults. Maternal *ybx1*$^{tsu3d5i/tsu3d5i}$ (M*ybx1*) mutant embryos were collected by crossing Z*ybx1* females with wild-type (WT) males. As revealed by quantitative reverse transcription PCR (qRT-PCR) and whole-mount *in situ* hybridization (WISH), maternal *ybx1* transcripts in M*ybx1* embryos were largely eliminated, which was presumably caused by nonsense-mediated mRNA decay (Fig. 1B,C). Given the protein truncation and mRNA loss, we believe that *ybx1*^{tsu3d5i} is a null allele.

M*ybx1* mutant embryos exhibited pronounced morphological defects with complete penetrance (Fig. 1D). Opaque deposits were observed in mutant embryo yolk. In contrast to the orderly stacked blastomeres in WT embryos during the cleavage period, M*ybx1* blastomeres showed abnormal shapes and placement. M*ybx1* embryos failed to initiate epiboly and displayed two classes of morphological phenotypes starting from around 4 h postfertilization (hpf). Class I embryos, usually comprising 20%-35% of a batch, had a relatively clear border between the blastoderm and the yolk. In contrast, the blastoderm in Class II embryos intermingled with the yolk (Fig. 1D). M*ybx1* embryos died gradually, when time-matched WT embryos underwent gastrulation and segmentation. MZ*ybx1* embryos obtained from crosses between homozygous mutant fish were morphologically similar to M*ybx1* embryos. Embryos obtained by crossing WT females with homozygous mutant males were normal. The M*ybx1* defects could be substantially rescued by maternally expressed GFP-Ybx1 fusion protein in M*ybx1*; *Tg(ef1α:GFP-ybx1)* embryos, confirming the causal relationship between the defects and maternal *ybx1* disruption (Fig. 1E). Taking these data together, we conclude that maternal, but not zygotic, *ybx1* is indispensable for zebrafish embryonic development.

Characterization of pleiotropic defects in M*ybx1* mutants

In addition to cleavage and gastrulation defects, we also found that M*ybx1* embryos at the one-cell stage showed shortened chorion elevation distance that manifested the egg activation defect (Fig. 2A,B). To further analyze the activation phenotype of mutant eggs, we studied two events that are tightly associated with egg activation: cortical granule (CG) exocytosis and cytoplasmic streaming (Fuentes and Fernández, 2010; Hart, 1990; Li-Villarreal et al., 2015). We labelled CGs using fluorescein-conjugated *Maclura pomifera* lectin to assess CG exocytosis in activated eggs (Becker and Hart, 1999; Dosch et al., 2004). Compared with WT eggs, mutant eggs had abundantly retained CGs (Fig. 2C). We also injected rhodamine dye into WT and M*ybx1* embryo yolk after fertilization to observe the cytoplasmic streaming. In WT embryos, vigorous cytoplasmic movement toward the animal pole was recorded (Movie 1). In contrast, M*ybx1* embryos showed stagnant cytoplasmic streaming (Movie 2). These results conclude the egg activation defect in *ybx1* mutants.

The appearance of embryonic abnormality in M*ybx1* mutants immediately after fertilization suggested defective oogenesis. Thus, we sought to observe *ybx1* mutant oocytes isolated from Z*ybx1* females. We sacrificed WT and Z*ybx1* female fish at 10 days post-purging (dpp), when WT oocytes mature to stages III and IV predominantly (Nair et al., 2013). Z*ybx1* ovaries were typically smaller than WT ones (Fig. S1A). The *ybx1* mutant oocytes were capable of developing to stages III and IV, although showing relatively lower efficiency (Fig. S1B). WT and *ybx1* mutant oocytes had indistinguishable appearances at stages III and IV (Fig. 2D). The translucency of ovulated WT stage-V eggs is a well-established hallmark of oocyte maturation. In contrast, prominent opaqueness was seen in *ybx1* mutant eggs (Fig. 2D). In addition, WT late stage-III and stage-IV oocytes could efficiently mature to stage V under 17α,20β-dihydroxy-4-pregnen-3-one (17α,20β-DHP) treatment *in vitro* (Fig. 2E) (Seki et al., 2008; Xu et al., 2014). The *ybx1* mutant oocytes exhibited reduced translucency after 17α,20β-DHP treatment, reflecting compromised maturation *in vitro* (Fig. 2E). Similarly, *in vivo* 17α,20β-DHP treatment of female fish is sufficient to induce oocyte maturation and ovulation (Tokumoto et al., 2011). The ovulated *ybx1* mutant eggs after *in vivo* 17α,20β-DHP treatment also manifested the egg activation defect (Fig. S2A,B). During the oocyte maturation from stage IV to V, the major yolk proteins undergo cleavage, which leads to the translucency (Dosch et al., 2004). We determined the yolk protein cleavage level by the ratio between the higher and lower molecular weight yolk proteins (HYP and LYP), displayed by SDS-PAGE and Coomassie staining. In WT and *ybx1* mutant stage-III/IV oocytes, the HYP/LYP ratios were similar. However, the ratio was more greatly decreased in WT stage-V eggs than in mutants (Fig. 2F). A similar phenomenon was also observed during *in vitro* maturation of oocytes (Fig. 2G). These results imply the deficiency of yolk protein cleavage during maturation of *ybx1* mutant oocytes. Therefore, we conclude that Ybx1 depletion impairs oocyte

Development (2018) 145, dev166587. doi:10.1242/dev.166587

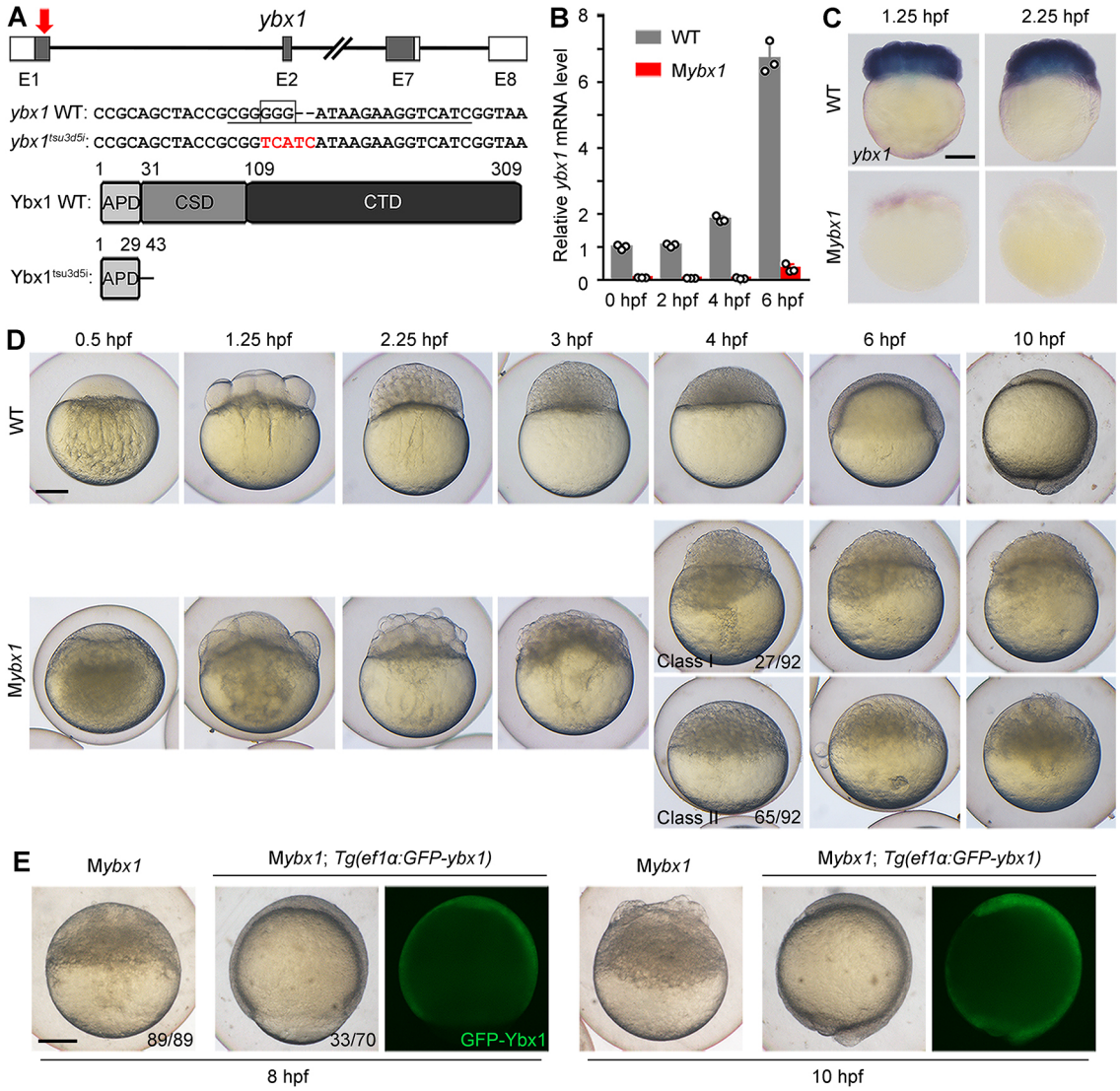

Fig. 1. Maternal *ybx1* mutant embryos exhibit severe morphological defects. (A) Generation of the *ybx1* mutant allele using CRISPR/Cas9. Top: the gRNA target site (red arrow) within the first exon (E1). Grey boxes, white boxes and connecting lines represent the open reading frame, untranslated regions and introns, respectively. Middle: sequences of *ybx1* WT and *ybx1*^{tsu3d5i} alleles near the gRNA target site (underlined) showing the deleted 3 bp (boxed) and the 5-bp insertion (red). Bottom: domains of Ybx1 WT protein and predicted mutant protein. APD, alanine/proline-rich domain; CSD, cold shock domain; CTD, C-terminal domain. (B,C) Loss of *ybx1* mRNA in M*ybx1* embryos revealed by qRT-PCR (B) and WISH (C). (D) Bright-field images showing the embryonic malformation of M*ybx1* mutants in contrast to time-matched WT embryos. (E) Bright-field and fluorescent images of M*ybx1* embryos expressing GFP-Ybx1. M*ybx1*; *Tg(ef1α:GFP-ybx1)* embryos were obtained by crossing Z*ybx1*; *Tg(ef1α:GFP-ybx1)* females to WT males. Scale bars: 200 µm.

maturation through stage V, which cannot be rescued by supplementing maturation hormone.

To characterize the cellular basis of morphological defects observed in M*ybx1* embryos, we next analyzed some fundamental cellular structures. DAPI staining unveiled pronounced fragmentation of nuclei in M*ybx1* mutants (Fig. 2H-J). The nuclear pore complex (NPC) in the nuclear envelope could be observed by immunostaining using the NPC antibody Mab414 in WT but not mutant embryos (Fig. 2J). In addition, plasma membrane structure and furrow formation were demolished in M*ybx1* embryos, as indicated by membrane β-catenin immunofluorescence (Fig. 2K,L). α-Tubulin networks connecting the yolk and blastomeres were formed in WT embryos, but not in M*ybx1* mutants (Fig. 2M). Taken together, these results reveal pleiotropic defects at the cellular level in M*ybx1* mutants during cleavage and blastulation.

Epiboly initiation requires Ybx1 protein translated after fertilization

Given the severe early defects, the phenotype manifested at later stages in M*ybx1* embryos may be the consequence of oogenesis and cleavage abnormalities and therefore does not confirm the postfertilization requirement of Ybx1, especially during blastulation and gastrulation. Therefore, we sought to generate Ybx1-depleted embryos with normal oogenesis and cleavage. To this end, we designed two translation-blocking morpholinos (*ybx1*-MO1 and *ybx1*-MO2) targeting *ybx1* mRNA 5′-UTR to knock down *ybx1*. Because a lower dose of *ybx1*-MO2 generated morphological changes that were similar to a higher dose of *ybx1*-MO1, we chose to inject 4 ng of *ybx1*-MO2 (yMO) in subsequent analyses (Fig. S3A). Injection of yMO at the one-cell stage markedly reduced Ybx1 protein level in gastrulas (Fig. S3B). In comparison with embryos that were injected with the control MO

Development (2018) 145, dev166587. doi:10.1242/dev.166587

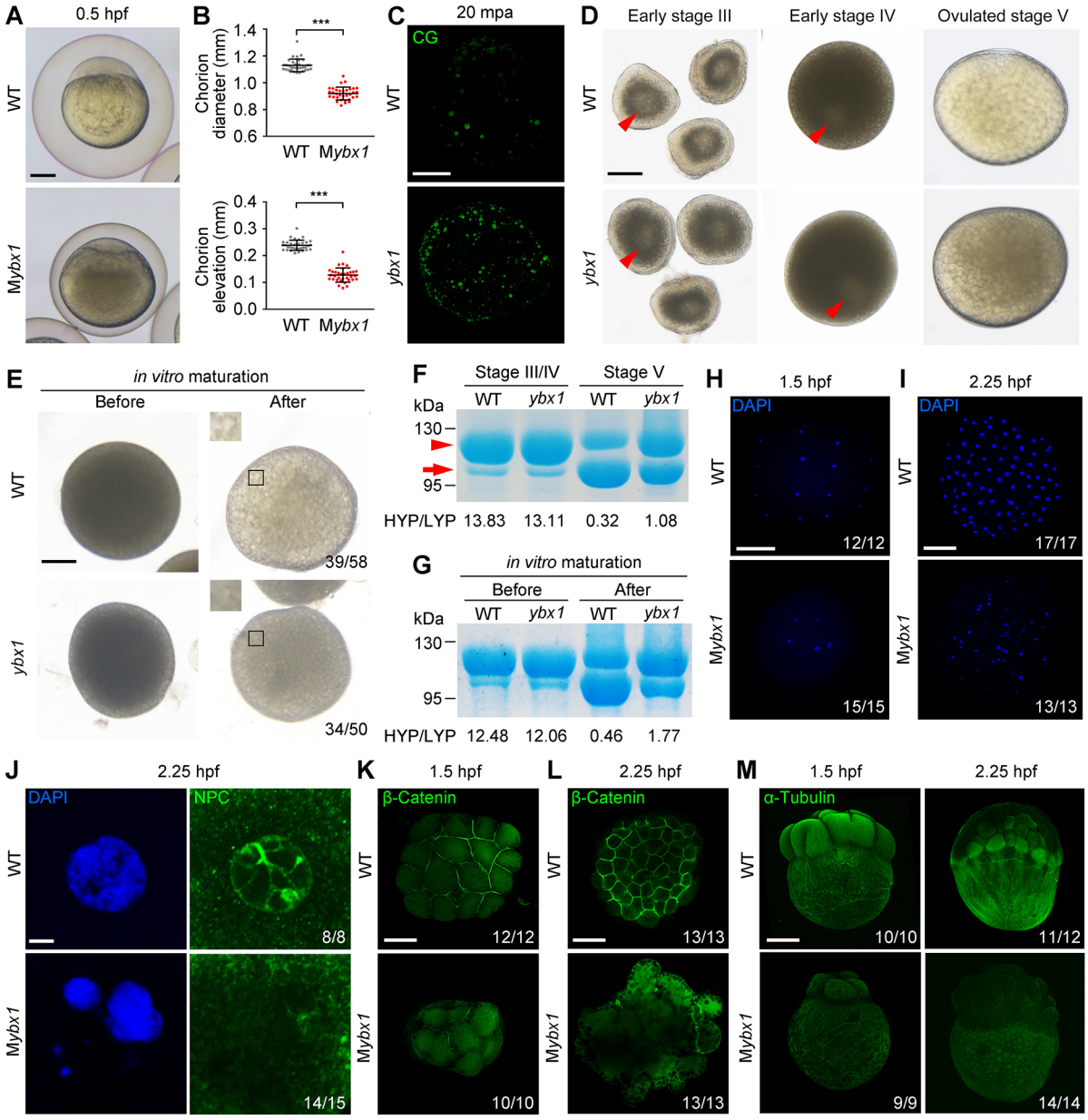

Fig. 2. Characterization of M*ybx1* mutant phenotype. (A) WT and M*ybx1* embryos with chorions at 0.5 hpf. (B) Measurement of chorion diameters and chorion elevation distances at 0.5 hpf. ***P<0.001; n=33; Welch's t-test. (C) Representative images showing labelling of cortical granules (CG) in WT and *ybx1* mutant eggs fixed at 20 min post-activation (mpa). Lateral views of eggs are shown. Eggs observed: WT n=23, mutant n=28. (D) Early stage-III oocytes, early stage-IV oocytes and ovulated stage-V eggs from WT and Z*ybx1* female fish. Arrowheads indicate germinal vesicles (oocyte nuclei) in the centre of stage-III oocytes and closer to the cortex in stage-IV oocytes. (E) WT and *ybx1* mutant oocytes before and after *in vitro* maturation. Insets show enlarged regions of the yolk. Relative opaqueness is seen in *ybx1* mutants. (F) SDS-PAGE and Coomassie staining of major yolk proteins of stage-III/IV oocytes and stage-V eggs. The higher and lower molecular weight yolk proteins (HYP and LYP) are indicated by the arrowhead and arrow, respectively. HYP/LYP ratios were calculated to represent yolk protein cleavage levels. (G) Major yolk protein cleavage in oocytes before and after *in vitro* maturation. Three independent experiments were performed for F and G. (H,I) Whole-mount DAPI staining of WT and M*ybx1* embryos at 1.5 hpf (H) and 2.25 hpf (I) shown in animal pole views. (J) DAPI staining and NPC immunofluorescence in 2.25 hpf embryos. (K,L) β-Catenin membrane immunofluorescence in 1.5 hpf (K) and 2.25 hpf (L) embryos shown in animal pole views. (M) α-Tubulin immunofluorescence in 1.5 hpf and 2.25 hpf embryos shown in lateral views. Numbers of observations are indicated in H-M. H shows inverted fluorescence microscopic images. I,K,M show maximum intensity projections of confocal z-slices. J and L show individual confocal planes. Scale bars: 200 µm in A,C-E,H,I,K-M; 5 µm in J.

(cMO), *ybx1* morphants exhibited prominent epiboly arrest (Fig. 3A). yMO injection rendered the vast majority of embryos unable to initiate epiboly. The blastoderm of *ybx1* morphants bent to form a crescent shape but failed to engulf the yolk and spread toward the vegetal pole. To confirm that the morphant phenotype was caused by *ybx1* knockdown instead of non-specific effects of MO injection, we injected yMO into *Tg(ef1α:GFP-ybx1)* transgenic embryos, which have maternally overexpressed GFP-Ybx1 fusion protein encoded by the mRNA without the yMO targeting site. Epiboly was successfully restored in a considerable portion (34/55) of injected *Tg(ef1α:GFP-ybx1)* embryos, suggesting the specificity of the yMO knockdown effect (Fig. 3B).

Development (2018) 145, dev166587. doi:10.1242/dev.166587

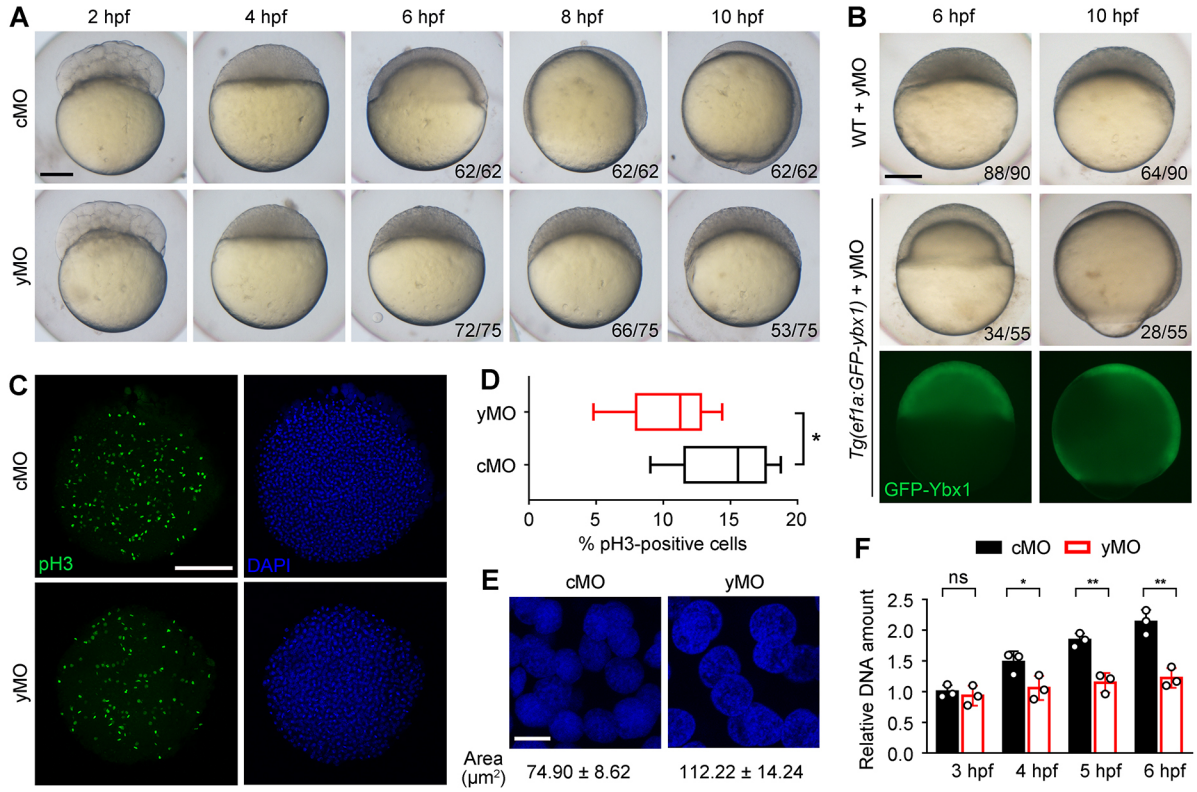

Fig. 3. Postfertilization production of Ybx1 is required for embryonic cell proliferation and epiboly initiation. (A) Bright-field images of embryos injected with cMO or yMO. Some yMO-injected embryos underwent yolk collapse and died, thus reducing the number of embryos with the representative phenotypes from 6 hpf to 10 hpf. (B) yMO-injected WT and *Tg(ef1α:GFP-ybx1)* embryos. Fluorescent images show the *GFP-ybx1* transgene expression driven by zebrafish *ef1α* promoter. (C) Labelling of pH3-positive cells in MO-injected embryos fixed at 4 hpf, with the quantification displayed by box-and-whisker plots in D. *P<0.05; n=9 regions of interest from three embryos; Student's t-test. (E) Confocal z-projections of DAPI staining. Measurement of the nucleus area is presented as mean±s.d. (n=20 nuclei). (F) Quantification of extracted genomic DNAs from equal numbers of cMO or yMO-injected embryos. Each circle represents the value of a sample containing ten embryos. ns, not significant; *P<0.05, **P<0.01; n=3; Student's t-test. Scale bars: 200 µm in A-C; 10 µm in E.

It appeared that the number of cells in *ybx1* morphants was reduced (Fig. 3A). Thus, we assessed cell proliferation by immunostaining the mitotic marker phospho-Histone H3 (pH3), which is typically positive in late G2-phase and M-phase cells (Fig. 3C) (Mendieta-Serrano et al., 2013). The total number and percentage of $pH3^+$ cells were reduced in yMO-injected embryos, indicating the presence of the cell proliferation defect (Fig. 3C,D). DAPI staining revealed that morphant embryos had larger cell nuclei, which can be induced by cell cycle arrest (Fig. 3E) (Yao et al., 2017). In accordance with impaired cell proliferation, the total amount of DNA was reduced in morphants compared with time-matched control embryos during epiboly (Fig. 3F). Therefore, inhibition of postfertilization production of Ybx1 leads to cell proliferation impairment and epiboly initiation failure. These data validate the embryonic requirement of Ybx1 for normal blastulation and gastrulation.

Interruption of the MZT in embryos depleted of Ybx1

To investigate the molecular foundation of the M*ybx1* mutant phenotype, we performed RNA sequencing (RNA-seq) analysis to obtain the transcriptome profiles of WT and M*ybx1* embryos at 0 hpf and 6 hpf. Ribosomal RNA depletion instead of poly(A) selection was used to enrich mRNAs in the samples, to avoid the influence of highly heterogeneous and variable poly(A) tail lengths in early embryos (Aanes et al., 2011; Subtelny et al., 2014). We first compared WT and mutant maternal transcriptomes in the one-cell-stage (0 hpf) embryos, as Y-box proteins have been shown to ubiquitously associate with maternal mRNAs in oocytes (Bouvet and Wolffe, 1994; Kohno et al., 2003). We analyzed 10,785 abundant maternal protein-coding mRNAs [>5 fragments per kilobase of transcript per million (FPKM) in either WT or M*ybx1* at 0 hpf]. The majority of them showed comparable maternal expression levels in WT and mutants (84.1% with <2-fold difference) (Fig. S4A). The qRT-PCR validation ruled out the possible impact of total mRNA quantity difference (Fig. S4B,C). Therefore, global mRNA instability was not found in 0 hpf M*ybx1* mutants. Considering the severe nuclear organization defect in M*ybx1* embryos, we specifically examined maternal expression of DNA damage response (DDR) genes based on the 0 hpf RNA-seq data. The levels of key DDR genes are comparable in WT and M*ybx1* embryos, suggesting that the maternal DDR programme is intact in mutants (Fig. S4D).

Given that the MZT progression associates with epiboly initiation (Lee et al., 2013; Zhao et al., 2017), we wondered whether the MZT is affected in M*ybx1* and morphant embryos. The MZT is an evolutionarily conserved event that is constituted by maternal transcript clearance and ZGA. To assess the maternal transcript clearance, 3205 unstable maternal mRNAs with >5 FPKM at 0 hpf and >75% FPKM decrease from 0 hpf to 6 hpf in WT embryos were analyzed. Plotting of mRNA level changes revealed that maternal mRNA degradation is impaired in M*ybx1* mutants. Unstable maternal mRNAs largely remained in post-MZT mutant embryos (Fig. 4A and Fig. S5A). qRT-PCR results confirmed that mRNA decay in M*ybx1* mutants, as well as in yMO-injected embryos, was

Development (2018) 145, dev166587. doi:10.1242/dev.166587

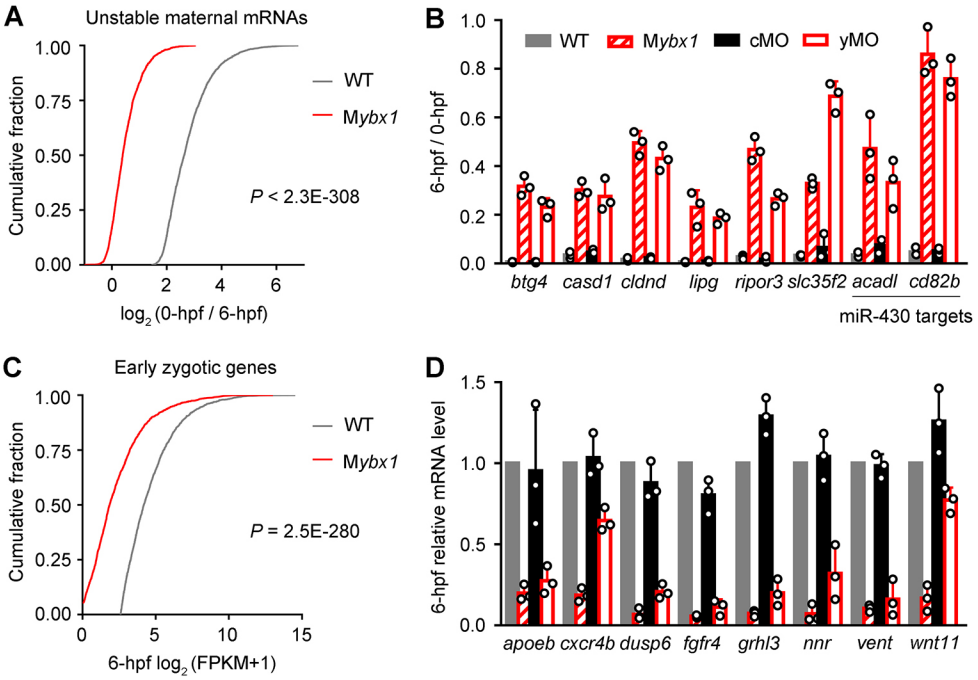

Fig. 4. Maternal Ybx1 is essential for the MZT. (A) Cumulative distributions of the maternal transcript decay levels (0 hpf/6 hpf, $\log_2$-scale) in WT and M*ybx1* embryos during the MZT. The plots show 3205 unstable maternal mRNAs. (B) qRT-PCR analysis of post-MZT levels (6 hpf/0 hpf) of representative unstable maternal mRNAs in WT, M*ybx1*, cMO- and yMO-injected embryos. Among the analyzed mRNAs, *acadl* and *cd82b* are miR-430 targets. (C) Cumulative distributions of 1818 early zygotic gene expression levels ($\log_2$-scale) in 6 hpf WT and M*ybx1* embryos. In A and C, FPKM+1 values were used for calculation to include genes with 0 FPKM. *P* values were determined by two-sided Wilcoxon rank sum tests. (D) qRT-PCR analysis of early zygotic gene expression in 6 hpf embryos. Fold changes were calculated with WT values set to 1. Each circle in B and D represents a normalized biological replicate result of qRT-PCR.

impaired (Fig. 4B). The stability of these mRNAs before MZT is not affected in M*ybx1* embryos (Fig. S5B). Among the mRNAs examined by qRT-PCR, *acadl* and *cd82b* are targets of zygotic microRNA miR-430, a key mediator of maternal transcript clearance (Giraldez et al., 2006). We extended our analysis by a comparison with previously published high-throughput data concerning miR-430 targets (Giraldez et al., 2006). We examined 176 identified miR-430 target mRNAs (see Materials and Methods for details). Among those, 138 (78.4%) showed reduced decay (>1.5-fold difference) from 0 hpf to 6 hpf in M*ybx1* mutants compared with WT embryos. Therefore, both miR-430-dependent and independent decay are affected in Ybx1-depleted embryos.

Similarly, we examined ZGA by analyzing 1818 early zygotic genes (>5 FPKM at 6 hpf and >4-fold increase from 0 hpf to 6 hpf in WT embryos). We noted that the vast majority (1516) of these genes have been shown to be upregulated (>twofold) during MZT in previously published RNA-seq datasets (Lee et al., 2013; Winata et al., 2018; Zhao et al., 2017). The expression levels of early zygotic genes were greatly downregulated in M*ybx1* embryos compared with WT at 6 hpf (Fig. 4C and Fig. S5C). The defects of ZGA in both M*ybx1* mutants and *ybx1* morphants were further confirmed by qRT-PCR (Fig. 4D). It has been established that several waves of gene induction occur during ZGA (Lee et al., 2013). We found that 94 out of 1567 early zygotic genes with a >2-fold higher level in 6 hpf WT than in M*ybx1* embryos belong to a total of 191 protein-coding first-wave genes defined by Lee et al. (2013). Therefore, different waves of gene activation are impaired by maternal Ybx1 loss. As miR-430 is zygotically expressed, the ZGA defect in Ybx1-depleted embryos could also contribute to the interruption of miR-430-dependent decay. Together, RNA-seq data and qRT-PCR validation demonstrate that the MZT process, composed of maternal mRNA decay and ZGA, is largely abolished in Ybx1-depleted embryos.

Elevated global translation in embryos depleted of Ybx1

Our phenotype and transcriptome analyses have established the crucial role of maternal Ybx1. We further explored how Ybx1 exerts its function. Ybx1 has been recognized as both an RNA-binding and DNA-binding protein that is mainly involved in translational repression, RNA stabilization and transcriptional regulation (Evdokimova et al., 2001; Holm et al., 2002; Kohno et al., 2003; Svitkin et al., 2009). GFP-Ybx1 expressed in oocytes is not localized to the nucleus, suggesting the unlikely involvement of Ybx1 in maternal gene transcription (Fig. S6). Global transcript destabilization was not discovered through the transcriptome analysis in 0 hpf embryos (Fig. S4A).

Next, we sought to examine whether Ybx1 loss affects translation. Given the broad RNA-binding affinity known for Y-box proteins, we hypothesized that reporter mRNAs without specifically designed elements should be useful for analyzing translational efficiency. Thus, the GFP reporter mRNA that contains the common SV40 terminator sequence was injected into one-cell-stage WT and M*ybx1* embryos together with rhodamine dye. The injected embryos were imaged under a fluorescence microscope at later stages and fluorescence levels were measured (Fig. 5A). The rhodamine dye acted as the loading control for injection. Fluorescence measurement showed that the reporter translation level was significantly higher in M*ybx1* embryos (Fig. 5B,D). Similar translational upregulation was also recorded in yMO-injected embryos compared with cMO (Fig. 5C,D). Using western blotting analysis, we confirmed the increase of GFP reporter translation in Ybx1-depleted embryos (Fig. 5E,F). The qRT-PCR analysis revealed that the level of injected GFP reporter mRNA did not show a significant change from 2 hpf to 6 hpf in either WT or M*ybx1* embryos (Fig. S8A). Therefore, the increased reporter translation in mutants may not be ascribed to altered mRNA stability. To demonstrate whether the translational change is restricted to the GFP reporter, we injected firefly luciferase (Fluc) reporter mRNA and recombinant *Renilla* luciferase (Rluc) protein to perform a similar assay (Fig. 5E). The Rluc protein served as the loading control. The luciferase assay result showed that Fluc reporter translation was also increased in Ybx1-deficient conditions (Fig. 5G). The elevated translation of two distinct mRNA reporters suggests the likelihood of an increase in overall translation level.

Development (2018) 145, dev166587. doi:10.1242/dev.166587

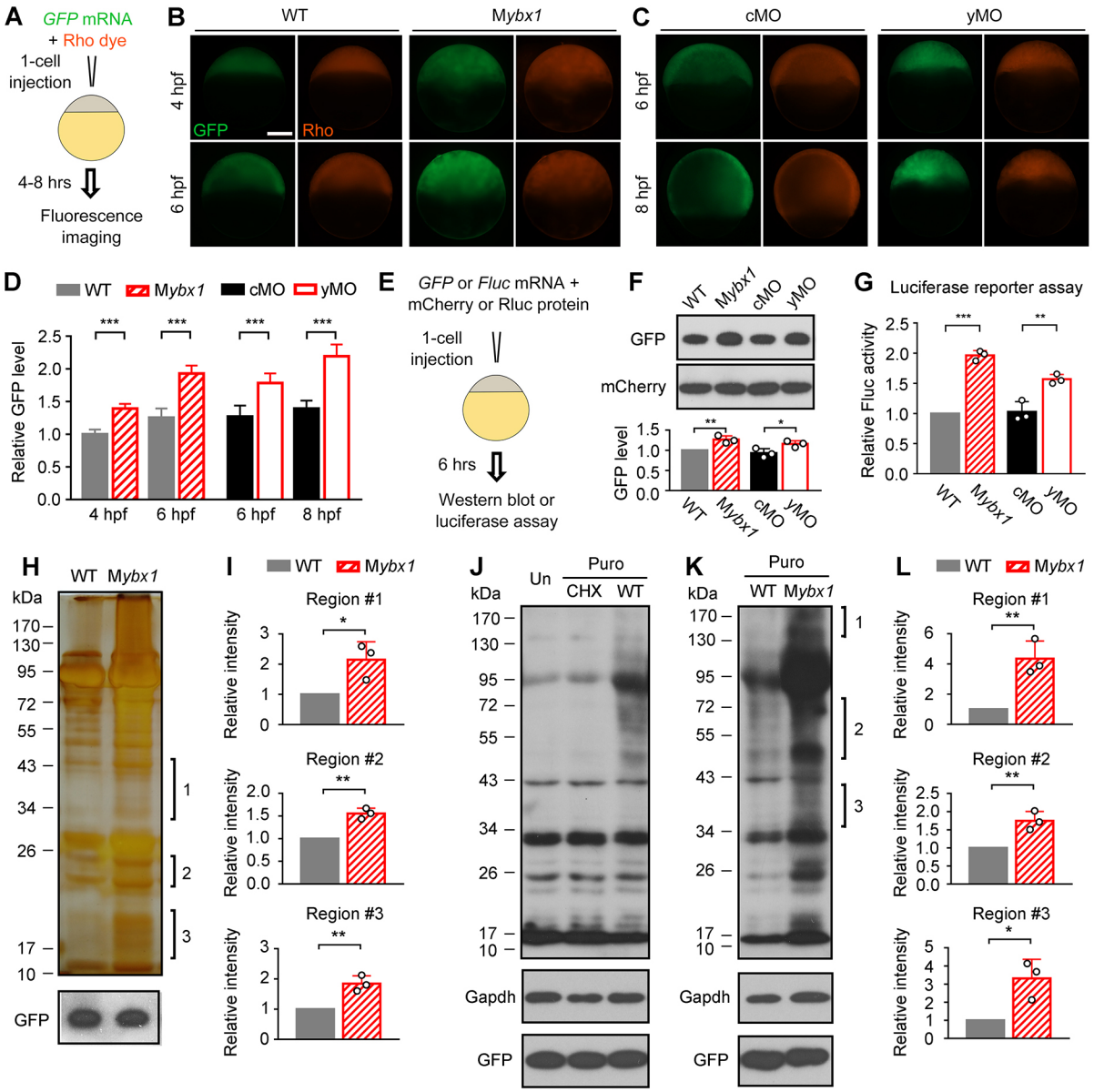

Fig. 5. Loss of maternal Ybx1 elevates global translation level. (A) Schematic of the fluorescent reporter translation assay. (B,C) Fluorescent images showing GFP reporter levels with rhodamine (Rho) control levels in WT, M*ybx1*, cMO- and yMO-injected live embryos at indicated stages. Scale bar: 200 µm. (D) Measurement of GFP reporter intensities relative to Rho. (E) Schematic of reporter translation assays using western blotting and luciferase assay. (F) Western blotting analysis of GFP reporter levels at 6 hpf. (G) Measurement of Fluc activities relative to Rluc. (H) SDS-PAGE and silver staining showing global protein levels in embryos. Three regions for measurement are indicated. 3 hpf embryos were lysed for the SDS-PAGE. GFP protein was injected at the one-cell stage as the loading control. (I) Quantification of relative signal intensities of three regions from H. (J) Western blot for the puromycin incorporation assay. GFP protein was injected as the loading control. Gapdh levels are also shown. Un, untreated; Puro, puromycin; CHX, cycloheximide. (K) Puromycin incorporation levels in WT and M*ybx1* embryos shown by western blotting. The injected GFP protein served as the loading control. (L) Relative puromycin signal intensities of three regions from western blots in K. **P*<0.05, ***P*<0.01, ****P*<0.001; ns, not significant; *n*=8 embryos for D, *n*=3 biological replicates for F,G,I,L; Student's *t*-test.

Next, we used SDS-PAGE and silver staining to assess global protein levels in embryos. To avoid the influence of impaired ZGA in M*ybx1* mutants, we harvested embryos at 3 hpf for analysis. Western blotting of injected recombinant GFP protein served as the loading control for SDS-PAGE. We observed a remarkable increase of protein quantities in M*ybx1* embryos (Fig. 5H). In order to visualize more protein bands, some bands were inevitably overdeveloped during silver staining because different proteins have vastly different quantities. We performed quantitative analysis of three regions in the gel with proper development. The result showed significantly upregulated protein levels in all three regions for M*ybx1* embryos (Fig. 5I). Similarly, we also observed an elevated global protein level in *ybx1* mutant eggs (Fig. S7A,B). In addition, we performed western blotting to check the endogenous protein levels of Gapdh and Khsrp, which were increased without mRNA level changes, in M*ybx1* embryos (Fig. S8B-D).

Furthermore, we employed the puromycin incorporation assay to examine the translation level in embryos (Schmidt et al., 2009). The embryos were treated with puromycin, which could be incorporated into newly synthesized polypeptide chains. Western blotting detection of incorporated puromycin is the output assessed to measure the global protein synthesis rate (Schmidt et al., 2009). The

Development (2018) 145, dev166587. doi:10.1242/dev.166587

puromycin-treated embryos exhibited stronger signals compared with untreated embryos or embryos treated with both puromycin and the translational blocker cycloheximide, verifying the feasibility of this approach (Fig. 5J). Stronger puromycin signals appeared for the M*ybx1* samples in comparison with WT samples (Fig. 5K). Similar to silver staining, three regions were selected for quantitative analysis to avoid possible non-specific bands. The result indicated elevated protein synthesis levels in M*ybx1* embryos (Fig. 5L). Taking the above data together, we conclude that Ybx1 is necessary for repressing global translation of maternal mRNAs during oocyte maturation and early embryonic development.

Ybx1 depletion induces the unfolded protein response

The endoplasmic reticulum (ER) functions as a crucial machinery for protein synthesis, modification and trafficking in eukaryotic cells. Cellular conditions that overwhelm the normal ER capacity, including massive protein misfolding and overloading, induce ER stress and the unfolded protein response (UPR), which potentially lead to cell death (Kaufman, 2002; Schröder and Kaufman, 2005). Therefore ER stress and the UPR are often associated with aberrant translational derepression (Kaufman, 2002; Miao et al., 2017). Given the global translation increase in embryos without Ybx1, we checked whether the excessive UPR also takes place. The splicing of *XBP1* mRNA has been established as a common indicator of ER stress (Back et al., 2005; Yoshida et al., 2001). Visualization of RNA-seq reads mapped to the *xbp1* gene showed prominent excision of the 26-bp intron in M*ybx1* embryos compared with WT embryos (Fig. 6A). We confirmed, by RT-PCR, the altered splicing of *xbp1* in both M*ybx1* and yMO-injected embryos (Fig. 6B,C). Moreover, expression of *atf3*, a central mediator of the UPR (Schröder and Kaufman, 2005), was upregulated in M*ybx1* and morphant embryos (Fig. 6D,E). Notably, 0 hpf M*ybx1* embryos also showed increased *atf3* expression, suggesting that the UPR is also triggered during oogenesis. These results indicate the existence of the excessive UPR in Ybx1-depleted embryos, which is presumably related to translational derepression and protein overloading.

Amelioration of M*ybx1* defects by supplementing translational repression

The above results have established the connection between maternal Ybx1 and translational repression. It remains unknown to what extent the translational derepression caused by Ybx1 loss is responsible for the observed defects. To address this issue, we tested whether adding a distinct translational repressor into M*ybx1* embryos could have a rescue effect. One ideal candidate is Eif4ebp1, the mammalian orthologue of which is known as 4E-BP1. It is an eIF4E inhibitor that negatively regulates cap-dependent translation (Pause et al., 1994). Mutations of two threonines to alanines render 4E-BP1 free of mTOR regulation and therefore constitutively active (CA) (Durand and Lykke-Andersen, 2013). We generated threonine-to-alanine substitutions at positions 34 and 43 of the zebrafish Eif4ebp1 to produce the CA form (Eif4ebp1-TTAA). We then constructed a transgenic line in which Eif4ebp1-TTAA is expressed under the control of the *ef1α* (*eef1a1l1*) promoter (Fig. S9A). Transgenic expression of Eif4ebp1-TTAA in WT background embryos led to general developmental delay without major morphological defects (Fig. S9B). This phenotype of delayed development is consistent with the role established for Eif4ebp1-TTAA in translational inhibition (Durand and Lykke-Andersen, 2013). We analyzed the M*ybx1*; *Tg(ef1α:GFP-Eif4ebp1-TTAA)* (M*ybx1*+TTAA) embryos, in which GFP-Eif4ebp1-TTAA was expressed in the absence of Ybx1 protein (Fig. 7A).

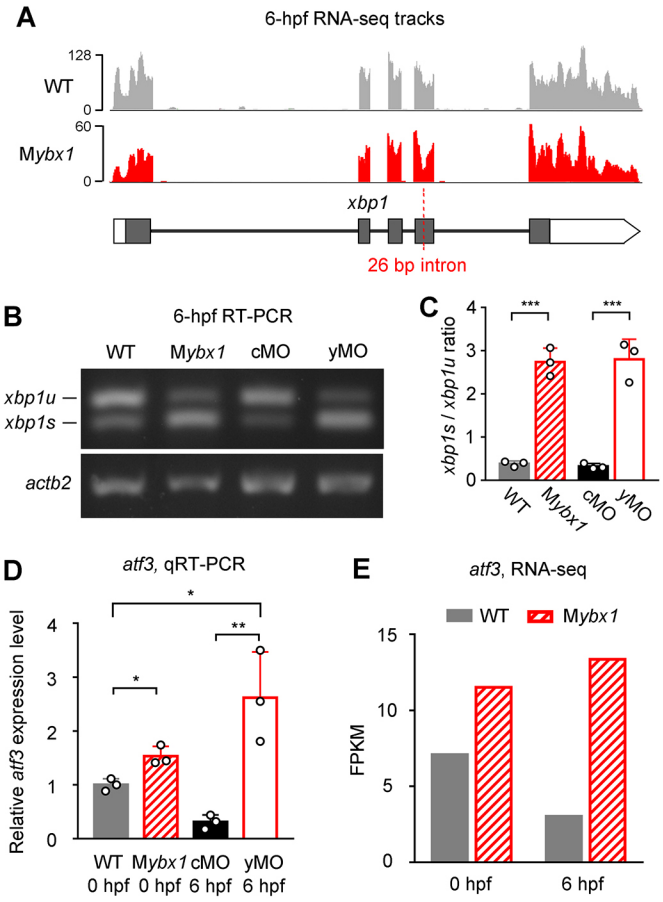

Fig. 6. Loss of maternal Ybx1 induces the UPR. (A) RNA-seq reads mapped to *xbp1* gene. Coverage tracks are displayed for WT and M*ybx1* embryos at 6 hpf. The 26-bp alternative intron related to the UPR is marked on the *xbp1* gene track. (B,C) RT-PCR examination of *xbp1* splicing. The increased amount of spliced *xbp1* (*xbp1s*) mRNA relative to unspliced *xbp1* (*xbp1u*) mRNA indicates excessive UPR in Ybx1-depleted embryos. *β-actin* (*actb2*) levels are also presented in B. The *xbp1s*/*xbp1u* ratio in C represents the intensity ratio of corresponding PCR product bands. (D) qRT-PCR analysis of *atf3* expression in response to Ybx1 depletion. (E) FPKM values of *atf3* expression in WT and M*ybx1* embryos at 0 hpf and 6 hpf. **P*<0.05, ***P*<0.01, ****P*<0.001; *n*=3; Student's *t*-test.

Significantly rescued egg activation of M*ybx1*+TTAA embryos could be observed after fertilization, indicated by increased chorion elevation (Fig. 7B-D) and promoted cytoplasmic streaming (Movie 3) in contrast to M*ybx1* mutants (Movie 2). Eif4ebp1-TTAA also improved the cleavage of major yolk proteins in eggs and in response to *in vitro* maturation (Fig. 7E,F). Importantly, a considerable portion of M*ybx1*+TTAA embryos were able to initiate epiboly, which was almost never seen in M*ybx1* mutants (Fig. 7G,H). The MZT process was also partially recovered in epiboly restored M*ybx1*+TTAA embryos, evidenced by decreased unstable maternal mRNAs and increased zygotically expressed mRNAs in post-MZT embryos (Fig. 7I,J). These results together suggest that Eif4ebp1-TTAA, as a translational repressor, confers a prominent rescue effect on M*ybx1* mutants. Therefore, translational repression constitutes a major part, if not all, of Ybx1 function in zebrafish embryos.

Translational repression by Ybx1 through the processing body

Y-box proteins are integral components of maternal mRNP particles found in *Xenopus* oocytes (Darnbrough and Ford, 1981; Dearsly

Development (2018) 145, dev166587. doi:10.1242/dev.166587

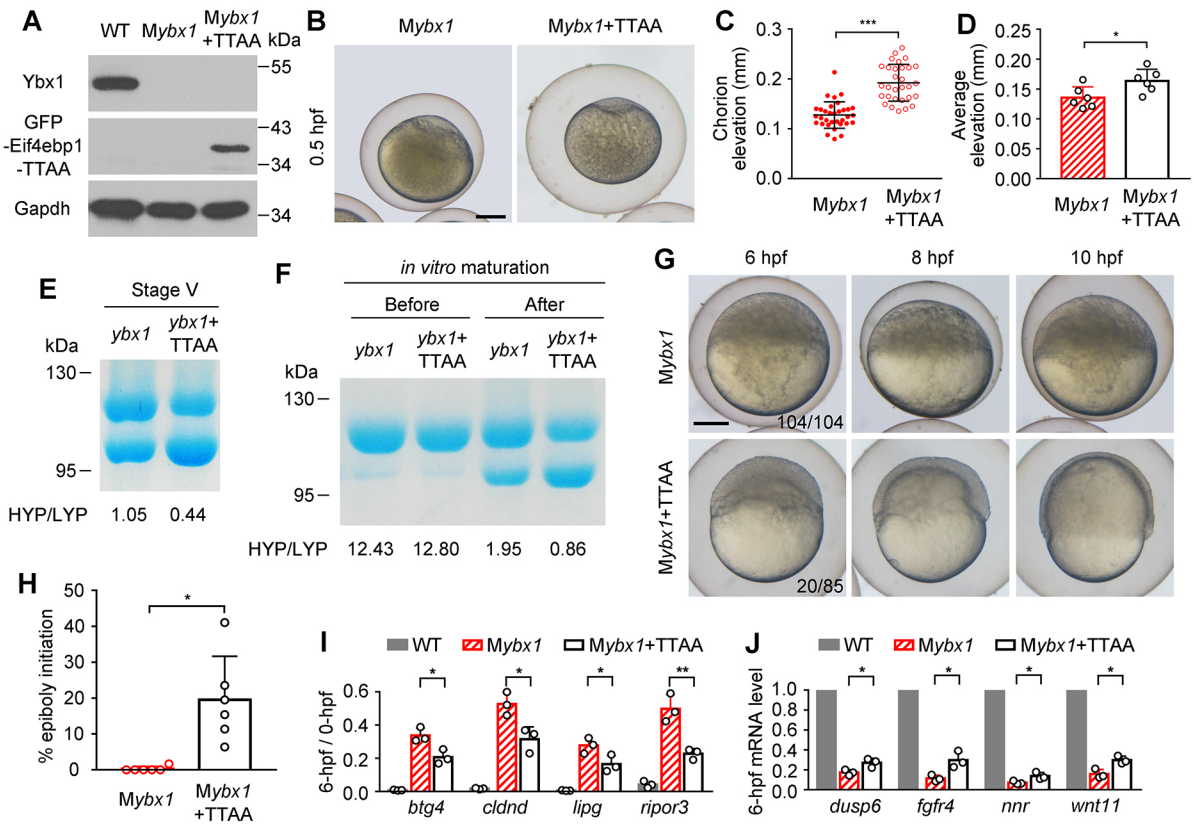

Fig. 7. Translational inhibition ameliorates the M*ybx1* phenotype. (A) Western blot of Ybx1, GFP-Eif4ebp1-TTAA and Gapdh protein expression in WT, M*ybx1* and M*ybx1*+TTAA embryos. (B) Bright-field images showing representative M*ybx1* and M*ybx1*+TTAA embryos with chorions after fertilization. (C) Chorion elevations of individual 0.5 hpf fertilized eggs from a single Z*ybx1* or Z*ybx1*+TTAA female. Each dot or circle represents one egg's value. ***P<0.001; Welch's t-test. (D) Average chorion elevations of fertilized eggs from different females. Six females of each group, 50-100 eggs per female, were analyzed. Each circle represents the average of all observed eggs from a single female. *P<0.05; Welch's t-test. (E) Coomassie staining of major yolk proteins of *ybx1* mutant and *ybx1*+TTAA stage-V eggs. HYP/LYP ratios were calculated to display yolk protein cleavage levels. (F) Major yolk protein cleavage in oocytes before and after *in vitro* maturation. (G) Bright-field images of M*ybx1* and M*ybx1*+TTAA gastrulas. (H) The percentage of epiboly restored M*ybx1*+TTAA embryos from different females. Epiboly initiation is extremely rare in M*ybx1* mutants. *P<0.05; n=6; Welch's t-test. (I,J) qRT-PCR detection of partially restored maternal mRNA clearance (I) and zygotic gene transcription (J) in M*ybx1*+TTAA embryos, compared with M*ybx1* mutants. WT results are also presented. *P<0.05, **P<0.01; n=3; Student's t-test. Scale bars: 200 µm.

et al., 1985; Deschamps et al., 1992; Murray et al., 1992). Because of the lack of a suitable antibody for immunostaining endogenous zebrafish Ybx1, we tried to look at subcellular localization of overexpressed HA-Ybx1 fusion protein in embryos. Interestingly, HA-Ybx1 proteins formed cytoplasmic foci when expressed in zebrafish embryos at 4 hpf (Fig. 8A,E). These structures were reminiscent of processing bodies (P-bodies), which are cytoplasmic protein aggregates involved in translational control and mRNA degradation (Decker and Parker, 2012). Previous studies have also reported the association of YBX1 with P-body components and its localization to RNA granules (Lyons et al., 2016; Somasekharan et al., 2015; Yang and Bloch, 2007). Therefore, we examined whether P-body components could also be found in Ybx1-containing foci in embryos. mRNAs encoding HA-Ybx1 and GFP-labelled P-body components Dcp1a or Patl1 were co-injected into one-cell-stage embryos. The imaging result showed that HA-Ybx1 and GFP-Dcp1a/Patl1 indeed colocalized in aggregates in embryonic cells at 4 hpf (Fig. 8A-H). Furthermore, endogenous Ybx1 can physically associate with GFP-Dcp1a, as revealed by co-immunoprecipitation (co-IP) in 8 hpf embryo lysates (Fig. 8I). Probably because of the limited protein product levels of injected mRNAs in earlier embryos, we were unable to detect colocalization and co-IP at pre-MZT stages. Overall, our results suggest that Ybx1 proteins may associate with P-body components and reside in P-body-like granules in early embryos.

We next asked whether the translational repression mediated by Ybx1 depends on its binding to individual mRNAs. The MS2-MCP system is employed to generate protein-RNA interaction (Bertrand et al., 1998). The multiple MS2 stem loops attached to specific RNA molecules are able to associate with designed MCP-tagged protein partners. We injected *GFP-24×MS2* mRNA, *mCherry* mRNA and blue-coloured Alexa Fluor 350 (AF350) dye into WT and M*ybx1* embryos. In line with the above results, both GFP and mCherry reporter translation levels were upregulated in M*ybx1* embryos compared with WT embryos (Fig. 8J,K). Additional input of HA-tagged tandem dimer MCP (HA-tdMCP), which possesses *GFP-24×MS2* mRNA binding ability, did not change either GFP or mCherry translation level in M*ybx1* embryos. In contrast, injection of the mRNA encoding HA-tdMCP-Ybx1, which directs Ybx1 to *GFP-24×MS2* mRNA, led to a significant decrease of the GFP reporter level. The mCherry level was decreased to a lesser extent, which might result from MCP-independent binding of HA-tdMCP-Ybx1 (Fig. 8J,K). These results suggest that tethering Ybx1 in proximity to the target mRNAs leads to promoted translational repression.

Development (2018) 145, dev166587. doi:10.1242/dev.166587

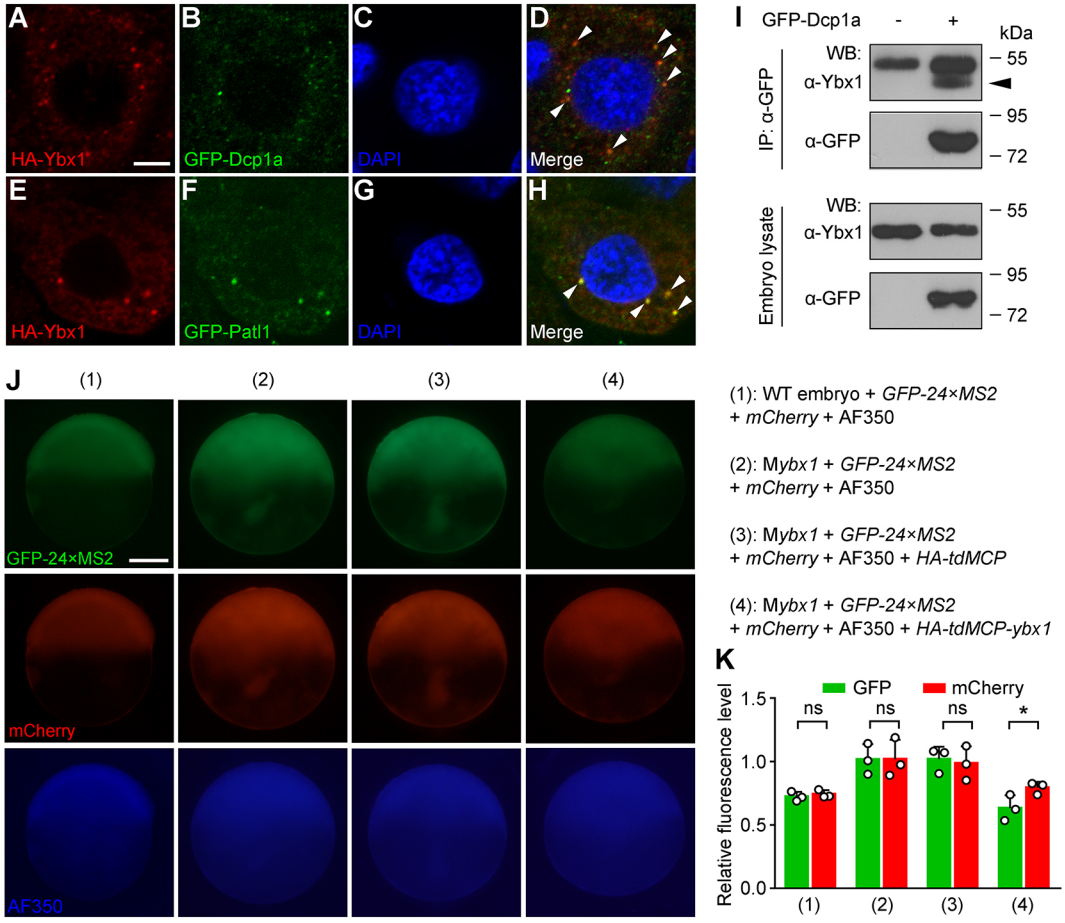

Fig. 8. Ybx1 is localized in P-body-like granules in embryos and represses the translation of bound mRNA. (A-H) Colocalization of HA-Ybx1 with the GFP-labelled P-body components Dcp1a (A-D) and Patl1 (E-H) in 4 hpf embryos. HA immunofluorescence (A,E), GFP immunofluorescence (B,F), DAPI staining (C,G) and merged signals (D,H) are shown in confocal slices. Arrowheads indicate colocalization foci. Scale bar: 5 µm. (I) Association of endogenous Ybx1 with GFP-Dcp1a in embryos revealed by co-IP. Embryos were injected with *gfp-dcp1a* mRNA at the one-cell stage and harvested at 8 hpf. IP, immunoprecipitation; WB, western blot. The arrowhead indicates the band of immunoprecipitated endogenous Ybx1 protein. (J) Fluorescent images showing the levels of GFP-24×MS2, mCherry and AF350 dye (loading control). Embryo genotypes and injected reagents are listed on the right. Scale bar: 200 µm. (K) Measurement of GFP and mCherry fluorescence levels relative to AF350. Both GFP and mCherry levels are upregulated in 2 and 3 compared with 1. Note the marked decrease of GFP intensity and the lesser decrease of mCherry in 4 compared with 3. ns, not significant; **P*<0.05; *n*=3 embryos; Student's *t*-test.

DISCUSSION

Ybx1, along with other Y-box binding proteins, has a long and complicated history of studies, shown by multiple names coined by different researchers. Because of its broad nucleic acid binding ability, it has been linked to various interacting partners and cellular processes. However, the *in vivo* roles of Y-box proteins, particularly in developmental processes, have not been well characterized using genetically modified animal models. In this study, we analyzed zebrafish Ybx1 function during early development using M*ybx1* null mutants. Our phenotypic characterization unveiled pleiotropic defects caused by the loss of maternal Ybx1, including impaired oocyte maturation, deficient egg activation, cellular malformations and abolition of the MZT. Considering the severe cellular defects, crucial cell activities, including chromosome segregation and cytoskeleton-mediated processes, may be largely affected in M*ybx1* mutants. Furthermore, arrest of cell cycle progression and epiboly movement in *ybx1* morphants implied the continuous requirement of Ybx1 protein supply during blastulation. In Ybx1-depleted embryos, we found aberrant translational upregulation and the excessive UPR, indicating the translational repression mediated by Ybx1. The amelioration of M*ybx1* defects by Eif4ebp1-TTAA validated the important role of Ybx1 as a translational repressor. We further showed the association of Ybx1 with P-body components, which are involved in mRNA silencing and decay. Taken together, these results delineate the mechanisms underlying the crucial role of maternal Ybx1 (Fig. 9).

One area of interest is whether epiboly failure and MZT loss in M*ybx1* mutants are caused by defective egg activation and cleavage. Given that knockdown of *ybx1* in WT embryos also impaired epiboly and the MZT without an influence on early cleavage (Fig. 3A), it is likely that later defects in M*ybx1* mutants are not necessarily secondary to the early defects. However, we cannot exclude the possibility that early defects aggravate later defects in M*ybx1* mutants.

The M$ybx1^{tsu3d5i}$ maternal mutant embryos we generated in this report exhibit anomalous cleavage and impaired epiboly, and deform during gastrulation or early segmentation (Fig. 1D).This is similar to the phenotypic appearance of M$ybx1^{sg8}$ mutant embryos reported by Kumari et al. (2013). However, careful examination indicates that M$ybx1^{tsu3d5i}$ oocytes undergo defective maturation with impaired yolk protein cleavage from stages IV to V (Fig. 2F,G) and the resulting fertilized eggs show abnormal egg activation (Fig. 2C) and cytoplasmic streaming (Movie 2). Our results support an idea that maternal Ybx1 protein starts to function before fertilization and is essential for ensuring egg quality. Any phenotypic differences

Development (2018) 145, dev166587. doi:10.1242/dev.166587

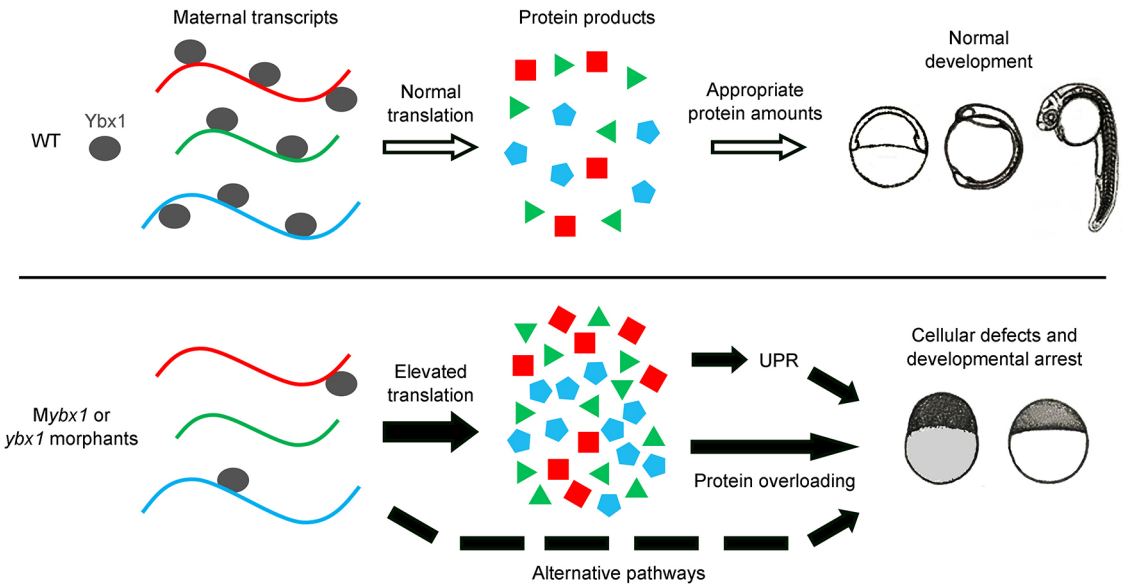

Fig. 9. The model for maternal Ybx1 function in zebrafish. Top: in WT embryos, Ybx1 functions as a general translational repressor. In cooperation with other translational regulators, Ybx1 maintains the correct level of global translation, ensuring appropriate amounts of proteins. Normal embryonic development is thus well supported. Bottom: in the absence of Ybx1, the balance of global translational control is jeopardized. Elevated translation leads to abnormally increased protein production. Both protein overloading itself, and the induced UPR, may cause severe cellular defects and developmental arrest. In addition, Ybx1 may also play roles through other potential alternative pathways.

among existing M*ybx1*^{tsu3d5i}, M*ybx1*^{sa42} and M*ybx1*^{sg8} mutants, if there are, might be explained by the different molecular nature of the mutations and/or the genetic backgrounds.

We uncovered the localization of overexpressed HA-Ybx1 fusion protein in P-body-like granules in zebrafish embryos (Fig. 8A-H). These observed granules may be homologous structures of stored mRNP particles in *Xenopus* oocytes. Both kinds of structures contain Y-box proteins and P-body components, and are functionally involved in maternal mRNA translational repression (Dearsly et al., 1985; Ladomery et al., 1997; Sommerville and Ladomery, 1996). Similar granules, for example the neuronal P-body-like granules, were also discovered in other types of cells (Barbee et al., 2006). Given the dispensability of zygotic *ybx1* in zebrafish somatic tissues, our findings raise the possibility that Y-box proteins are functionally required components of maternal mRNA granules, but not somatic granules. In agreement with this hypothesis, colocalization and physical association of Ybx1 with overexpressed P-body components were detected in post-MZT embryos. However, the results were not achieved with pre-MZT embryos, most likely because of relatively low levels of overexpressed proteins before MZT. Future efforts are needed to verify the existence of endogenous Ybx1-containing granules in oocytes and early embryos using optimized antibodies. Interestingly, as is seen with some other RNA granule proteins, YBX1 is able to form polymerized amyloid-like fibrils *in vitro* (Guryanov et al., 2012; Kato et al., 2012). It remains to be seen whether Ybx1 can also heavily polymerize in oocytes and embryos.

We noticed that Eif4ebp1-TTAA fails to fully rescue the M*ybx1* mutant phenotype (Fig. 7G). Therefore, we cannot exclude other potential pathways of Ybx1 functions in vertebrate oocytes and embryos (Fig. 9). For example, Ybx1 has been shown to regulate the processing of non-coding RNAs (Shurtleff et al., 2016, 2017; Wu et al., 2015). In the present study, we focused on protein-coding mRNAs in our RNA-seq analysis. It will be interesting to profile non-coding RNAs in M*ybx1* mutants. Another possibility underlying the partial rescue effect is that inappropriate levels of Eif4ebp1-TTAA may impact the rescue efficiency. Nevertheless, the pronounced rescue effect of Eif4ebp1-TTAA in M*ybx1* embryos establishes translational derepression as a primary cause of the severe phenotype.

The translational control is of particular importance in transcriptionally inactive early embryos, because of the lack of gene regulation at the transcription layer. Previous studies have provided numerous examples of how sequence-specific regulators shape translational levels of mRNAs containing targeted *cis*-regulatory elements (Chen et al., 2013; Sha et al., 2017; Tadros et al., 2007). In this study, we show that a relatively ubiquitous control mechanism also exists in oocytes and embryos to modulate translation. Furthermore, translation is globally activated following fertilization to support early embryogenesis (Bazzini et al., 2016). We demonstrate that maternal Ybx1 acts as a brake for this process and prevents protein overloading in embryos. Cooperation among diverse translational regulators ensures a proper protein synthesis level that carries the embryo through the MZT (Bazzini et al., 2016, 2012; Winata et al., 2018). Interestingly the MZT process itself, which is considered an event centred on RNA turnover, is also related to the switch of translational control modes (Schier, 2007; Subtelny et al., 2014; Winata et al., 2018). Our study highlights the presence of the Ybx1-dependent translational control module that is crucial for early embryonic development, but not required for later stages. Prospective mechanisms that also distinguish between early embryos and somatic cells will complete our knowledge of dynamic regulatory strategies during development.

MATERIALS AND METHODS

Zebrafish

Zebrafish husbandry and manipulation were approved by Tsinghua University Animal Care and Use Committee. Tuebingen strain zebrafish were used as WT fish and for generating genetically modified lines. Embryos were maintained in Holtfreter's solution at 28.5°C and staged according to the standard protocol (Kimmel et al., 1995).

To observe oocyte phenotype, ovaries were isolated from sacrificed female fish. Oocytes were immersed in oocyte culture medium [90%

Development (2018) 145, dev166587. doi:10.1242/dev.166587

Leibovitz's L-15 medium (Gibco), 0.5 mg/ml bovine serum albumin (Amresco), pH 9] for imaging. Oocyte maturation *in vitro* was achieved following a previously established protocol (Xu et al., 2014). Oocytes were incubated in oocyte maturation medium containing 17α,20β-DHP (Sigma-Aldrich) for 3 h before imaging. For hormone-induced oocyte maturation and ovulation *in vivo*, female fish were placed in 1 µg/ml 17α,20β-DHP for 4 h. Ovulated eggs were squeezed out by gently pressing the female fish abdomen.

CRISPR/Cas9-mediated mutagenesis was performed as previously reported (Chang et al., 2013; Yao et al., 2017). The guide RNA (gRNA) target site was selected with CHOPCHOP (Montague et al., 2014). The PCR primers used for T7 endonuclease I assay (ybx1-target-F, ybx1-target-R) and genotyping (ybx1-wt-F, ybx1-mut-F, ybx1-target-R) are listed in Table S1. Tol2-mediated transgenesis was performed using the previously described system (Han et al., 2011). A 347 bp promoter between −326 and +21 positions from the zebrafish *eef1a1l1* transcription start site was employed to drive transgene expression. For the generation of *Tg(ef1α:GFP-ybx1)* and *Tg(ef1α:GFP-Eif4ebp1-TTAA)* strains, the construct and *Tol2* mRNA were injected into WT embryos. For the generation of M*ybx1*; *Tg(ef1α:GFP-ybx1)* and M*ybx1*; *Tg(ef1α:GFP-Eif4ebp1-TTAA)* strains, the construct and mRNA were injected into embryos from crosses between homozygous mutant males and heterozygous females. The identified founder fish were crossed to obtain F1 fish for producing transgenic embryos.

mRNAs, morpholinos and recombinant proteins

Open reading frames were inserted into the pCS2+ vector for *in vitro* synthesis of mRNAs using the mMESSAGE mMACHINE SP6 kit (Thermo Fisher Scientific). The coding sequences for 24×MS2 and tdMCP are from Addgene plasmids #31865 and #40649 (deposited by Robert Singer), respectively (Bertrand et al., 1998; Wu et al., 2012). mRNA injection doses per embryo in this study are as follows: *GFP*, 100 pg; *Fluc*, 200 pg; *HA-ybx1*, 200 pg; *GFP-dcp1a*, 400 pg; *GFP-patl1a*, 500 pg; *GFP-24×MS2*, 300 pg; *mCherry*, 200 pg; *HA-tdMCP*, 200 pg; and *HA-tdMCP-ybx1*, 450 pg. Rhodamine dye (Sigma-Aldrich, R8881) was injected as the loading control or to visualize cytoplasmic movement.

The antisense morpholinos were purchased from Gene Tools. Sequences are as follows: *ybx1*-MO1, CTCTCTAGTGTGTTTTCCCGGTGCT; *ybx1*-MO2 (yMO), CGGCCTCGCTGCTCATGTTGTTTTC; control MO (cMO), TAATTTACTTACCCTCAAGTTGCTG.

Recombinant protein expression and purification were performed as previously described (Liu et al., 2013). Sequences encoding Rluc, GFP and mCherry were cloned into the pGEX-6P-1 vector for GST-labelled protein expression. Transformed BL21-competent *Escherichia coli* cells were cultured and Glutathione Sepharose 4B (GE Healthcare) was used for protein purification. The loading control was a 50 pg injection of Rluc, GFP or mCherry protein.

Whole-mount *in situ* hybridization and immunofluorescence

Whole-mount *in situ* hybridization and immunofluorescence were performed following standard protocols as previously described (Liu et al., 2013; Xu et al., 2014). The digoxigenin-labelled antisense probe was synthesized using the DIG RNA labelling kit (Roche). Anti-Digoxigenin-AP antibody (Roche, 11093274910, 1:3000) and BM Purple AP substrate (Roche) were used for hybridization signal detection. Primary antibodies that were used for immunofluorescence were: anti-NPC proteins (Abcam, ab24609, 1:1000), anti-β-catenin (Sigma-Aldrich, C2206, 1:1000), anti-α-tubulin (Sigma-Aldrich, T6199, 1:400), anti-pH3 (Cell Signaling Technology, 9701, 1:200), anti-HA (Santa Cruz Biotechnology, sc-7392, 1:200) and anti-GFP (Abcam, ab13970, 1:500). Secondary antibodies were: Alexa Fluor 488 goat anti-mouse IgG (Jackson ImmunoResearch, 115-545-003, 1:200), Alexa Fluor 488 goat anti-rabbit IgG (Jackson ImmunoResearch, 111-545-003, 1:200), Alexa Fluor 647 goat anti-mouse IgG (Jackson ImmunoResearch, 115-605-003, 1:200), and Alexa Fluor 488 goat anti-chicken IgY (Abcam, ab150169, 1:200). Cortical granules were labelled using fluorescein-conjugated *Maclura pomifera* lectin (Vector Laboratories, FL-1341) as previously reported (Becker and Hart, 1999).

Microscopy

For morphological phenotype capture, embryos were maintained in Holtfreter's solution and photographed using a Nikon SMZ1500 stereomicroscope. For images showing WISH results, stained embryos were immersed in glycerol and photographed under the stereomicroscope. Live embryos and oocytes were photographed under an Olympus MVX10 fluorescence microscope for epifluorescent images. Confocal images were acquired using a Zeiss 710 or Zeiss 710 META confocal microscope. ImageJ software (http://imagej.nih.gov/ij/) was used for image analyses, including fluorescence intensity measurement, length measurement, area measurement and cell counting. When assessing chorion elevation distances, embryo and chorion diameters were first measured. The chorion elevation was calculated by 0.5×(chorion diameter−embryo diameter).

qRT-PCR, DNA quantification and luciferase assay

Total RNA was extracted from embryo samples using TRIzol reagent (Thermo Fisher Scientific). RNA was treated with DNase I (Tiangen Biotech) and further purified with RNeasy Mini kit (Qiagen). cDNA was generated by reverse-transcribing 1 µg of total RNA with M-MLV reverse transcriptase (Promega) and random hexamers (Promega). Quantitative PCR was performed using a Roche LightCycler 480 machine and analyzed following the $2^{-\Delta\Delta Ct}$ method. Unless otherwise noted, *vasa* was used as the reference gene for qRT-PCR because of its approximately equal expression levels in WT and mutants and relative stability in early embryos. Primers that were used for qRT-PCR and RT-PCR experiments are listed in Table S2. Genomic DNA quantification of embryos was performed in reference to the previously reported method (Zhao et al., 2017). Luciferase reporter assay for embryo lysates was carried out as previously described for mammalian cell samples (Liu et al., 2013).

RNA-seq and analysis

Total RNA extraction and genomic DNA clearance were carried out as stated above. To further purify mRNA, samples were treated with NEBNext rRNA depletion kit (New England Biolabs) to eliminate rRNA. Sequencing libraries were constructed with NEBNext Ultra RNA Library Prep Kit for Illumina (New England Biolabs). Clustered library preparations were sequenced on an Illumina HiSeq 2500 machine and 50 bp single-end reads were generated. Clean reads, with low quality reads removed from the raw data, were mapped to the zebrafish GRCz10 reference genome using TopHat v2.0.12 (Trapnell et al., 2009). HTSeq v0.6.1 was employed to count the reads mapped to individual genes (Anders et al., 2015). FPKM values were then calculated to determine gene expression levels. Gene type information was acquired from Ensembl BioMart (http://www.ensembl.org/biomart) and only protein-coding genes were included for the transcriptome analysis in this study.

The previously published datasets were obtained from NCBI Gene Expression Omnibus for analyses. The miR-430 targets we analyzed are those mRNAs that have stable Ensembl gene IDs, contain miR-430 target sequence GCACUU in their 3′-UTRs, and are upregulated >1.5-fold in post-MZT MZ*dicer* embryos compared with WT and miR-430-injected MZ*dicer* embryos (Giraldez et al., 2006). For ZGA analysis, out of 269 first-wave genes that have been reported by Lee et al. (2013), we focused on 191 protein-coding ones according to BioMart gene information (Lee et al., 2013).

SDS-PAGE and puromycin incorporation assay

SDS-PAGE, silver staining and Coomassie staining were performed following the established protocol (Schägger, 2006). For each sample of the yolk protein cleavage assay, ten eggs were dechorionated and lysed in 500 µl TNE buffer [10 mM Tris-HCl (pH 7.4), 150 mM NaCl, 5 mM EDTA, 1% Triton X-100]. An aliquot of 5-10 µl lysate was loaded for SDS-PAGE and Coomassie staining. For puromycin incorporation assay, dechorionated embryos were treated with 50 µg/ml puromycin (Solarbio) from 2 hpf to 3 hpf. When necessary, cycloheximide was added 30 min before puromycin administration and remained at a concentration of 50 µg/ml until embryo lysis. Embryos were lysed at 3 hpf in TNE buffer and subjected to western blotting. Intensity measurement was carried out using ImageJ.

Development (2018) 145, dev166587. doi:10.1242/dev.166587

Western blotting and immunoprecipitation

Western blotting and immunoprecipitation were carried out essentially as previously described (Liu et al., 2013). For detection of puromycin incorporation, ECL plus super sensitive chemiluminescent substrate (Solarbio) was used. The following antibodies acted as primary antibodies for western blotting: anti-YBX1 (Sigma-Aldrich, WH0004904M1, 1:500), anti-GAPDH (ZSGB-Biotech, TA-08, 1:2000), anti-KHSRP (Sigma-Aldrich, SAB2101240, 1:500), anti-puromycin (Merck Millipore, MABE434, 1:5000), anti-GFP (Santa Cruz Biotechnology, sc-9996, 1:1000), anti-mCherry (Easy Bio, BE2026, 1:1000). For co-IP, injected embryos were lysed at 8 hpf in TNE buffer for further procedures. Anti-GFP (Santa Cruz Biotechnology, sc-9996, 1:100) antibody was used for immunoprecipitation.

Statistics

GraphPad Prism 7 was used for making statistical graphs and analyses. Wilcoxon rank sum tests were performed manually in Microsoft Excel. Error bars represent mean±s.d. unless otherwise noted. Sample sizes and statistical methods are specified in figure legends. All Student's and Welch's *t*-tests are unpaired, and all *P* values are two-sided.

Acknowledgements

We thank other members of the Meng laboratory for discussions, Robert Singer and Qiang Wang for sharing reagents, and the staff at the Center of Biomedical Analysis of Tsinghua University for technical assistance.

Competing interests

The authors declare no competing or financial interests.

Author contributions

Conceptualization: J.S., A.M.; Methodology: J.S., W.S., A.M.; Validation: J.S., A.M.; Formal analysis: J.S., L.Y., A.M.; Investigation: J.S., L.Y., W.S.; Writing - original draft: J.S.; Writing - review & editing: J.S., L.Y., A.M.; Visualization: J.S.; Supervision: A.M.; Project administration: A.M.; Funding acquisition: A.M.

Funding

This work was financially supported by the National Natural Science Foundation of China (31590832 to A.M.).

Data availability

RNA-seq data in this study have been deposited in NCBI Gene Expression Omnibus with accession number GSE108924.

Supplementary information

Supplementary information available online at
http://dev.biologists.org/lookup/doi/10.1242/dev.166587.supplemental

References

Aanes, H., Winata, C. L., Lin, C. H., Chen, J. P., Srinivasan, K. G., Lee, S. G. P., Lim, A. Y. M., Hajan, H. S., Collas, P., Bourque, G. et al. (2011). Zebrafish mRNA sequencing deciphers novelties in transcriptome dynamics during maternal to zygotic transition. *Genome Res.* **21**, 1328-1338.

Abrams, E. W. and Mullins, M. C. (2009). Early zebrafish development: it's in the maternal genes. *Curr. Opin. Genet. Dev.* **19**, 396-403.

Anders, S., Pyl, P. T. and Huber, W. (2015). HTSeq–a Python framework to work with high-throughput sequencing data. *Bioinformatics* **31**, 166-169.

Back, S. H., Schröder, M., Lee, K., Zhang, K. and Kaufman, R. J. (2005). ER stress signaling by regulated splicing: IRE1/HAC1/XBP1. *Methods* **35**, 395-416.

Barbee, S. A., Estes, P. S., Cziko, A.-M., Hillebrand, J., Luedeman, R. A., Coller, J. M., Johnson, N., Howlett, I. C., Geng, C., Ueda, R. et al. (2006). Staufen- and FMRP-containing neuronal RNPs are structurally and functionally related to somatic P bodies. *Neuron* **52**, 997-1009.

Bazzini, A. A., Lee, M. T. and Giraldez, A. J. (2012). Ribosome profiling shows that miR-430 reduces translation before causing mRNA decay in zebrafish. *Science* **336**, 233-237.

Bazzini, A. A., Del Viso, F., Moreno-Mateos, M. A., Johnstone, T. G., Vejnar, C. E., Qin, Y., Yao, J., Khokha, M. K. and Giraldez, A. J. (2016). Codon identity regulates mRNA stability and translation efficiency during the maternal-to-zygotic transition. *EMBO J.* **35**, 2087-2103.

Becker, K. A. and Hart, N. H. (1999). Reorganization of filamentous actin and myosin-II in zebrafish eggs correlates temporally and spatially with cortical granule exocytosis. *J. Cell Sci.* **112**, 97-110.

Bertrand, E., Chartrand, P., Schaefer, M., Shenoy, S. M., Singer, R. H. and Long, R. M. (1998). Localization of ASH1 mRNA particles in living yeast. *Mol. Cell* **2**, 437-445.

Bouvet, P. and Wolffe, A. P. (1994). A role for transcription and FRGY2 in masking maternal mRNA within Xenopus oocytes. *Cell* **77**, 931-941.

Chang, N., Sun, C., Gao, L., Zhu, D., Xu, X., Zhu, X., Xiong, J.-W. and Xi, J. J. (2013). Genome editing with RNA-guided Cas9 nuclease in zebrafish embryos. *Cell Res.* **23**, 465-472.

Chen, J., Torcia, S., Xie, F., Lin, C.-J., Cakmak, H., Franciosi, F., Horner, K., Onodera, C., Song, J. S., Cedars, M. I. et al. (2013). Somatic cells regulate maternal mRNA translation and developmental competence of mouse oocytes. *Nat. Cell Biol.* **15**, 1415-1423.

Darnbrough, C. H. and Ford, P. J. (1981). Identification in Xenopus laevis of a class of oocyte-specific proteins bound to messenger RNA. *Eur. J. Biochem.* **113**, 415-424.

Dearsly, A. L., Johnson, R. M., Barrett, P. and Sommerville, J. (1985). Identification of a 60-kDa phosphoprotein that binds stored messenger RNA of Xenopus oocytes. *Eur. J. Biochem.* **150**, 95-103.

Decker, C. J. and Parker, R. (2012). P-bodies and stress granules: possible roles in the control of translation and mRNA degradation. *Cold Spring Harb. Perspect. Biol.* **4**, a012286.

De Robertis, E. M. and Kuroda, H. (2004). Dorsal-ventral patterning and neural induction in Xenopus embryos. *Annu. Rev. Cell. Dev. Biol.* **20**, 285-308.

Deschamps, S., Viel, A., Garrigos, M., Denis, H. and le Maire, M. (1992). mRNP4, a major mRNA-binding protein from Xenopus oocytes is identical to transcription factor FRGY2. *J. Biol. Chem.* **267**, 13799-13802.

Didier, D. K., Schiffenbauer, J., Woulfe, S. L., Zacheis, M. and Schwartz, B. D. (1988). Characterization of the cDNA encoding a protein binding to the major histocompatibility complex class II Y box. *Proc. Natl. Acad. Sci. USA* **85**, 7322-7326.

Dosch, R., Wagner, D. S., Mintzer, K. A., Runke, G., Wiemelt, A. P. and Mullins, M. C. (2004). Maternal control of vertebrate development before the midblastula transition: mutants from the zebrafish I. *Dev. Cell* **6**, 771-780.

Durand, S. and Lykke-Andersen, J. (2013). Nonsense-mediated mRNA decay occurs during eIF4F-dependent translation in human cells. *Nat. Struct. Mol. Biol.* **20**, 702-709.

Edson, M. A., Nagaraja, A. K. and Matzuk, M. M. (2009). The mammalian ovary from genesis to revelation. *Endocr. Rev.* 30, 624-712.

Evdokimova, V. M., Wei, C.-L., Sitikov, A. S., Simonenko, P. N., Lazarev, O. A., Vasilenko, K. S., Ustinov, V. A., Hershey, J. W. B. and Ovchinnikov, L. P. (1995). The major protein of messenger ribonucleoprotein particles in somatic cells is a member of the Y-box binding transcription factor family. *J. Biol. Chem.* **270**, 3186-3192.

Evdokimova, V., Ruzanov, P., Imataka, H., Raught, B., Svitkin, Y., Ovchinnikov, L. P. and Sonenberg, N. (2001). The major mRNA-associated protein YB-1 is a potent 5′ cap-dependent mRNA stabilizer. *EMBO J.* **20**, 5491-5502.

Fuentes, R. and Fernández, J. (2010). Ooplasmic segregation in the zebrafish zygote and early embryo: pattern of ooplasmic movements and transport pathways. *Dev. Dyn.* **239**, 2172-2189.

Giraldez, A. J., Mishima, Y., Rihel, J., Grocock, R. J., Van Dongen, S., Inoue, K., Enright, A. J. and Schier, A. F. (2006). Zebrafish MiR-430 promotes deadenylation and clearance of maternal mRNAs. *Science* **312**, 75-79.

Goodarzi, H., Liu, X., Nguyen, H. C. B., Zhang, S., Fish, L. and Tavazoie, S. F. (2015). Endogenous tRNA-derived fragments suppress breast cancer progression via YBX1 displacement. *Cell* **161**, 790-802.

Guryanov, S. G., Selivanova, O. M., Nikulin, A. D., Enin, G. A., Melnik, B. S., Kretov, D. A., Serdyuk, I. N. and Ovchinnikov, L. P. (2012). Formation of amyloid-like fibrils by Y-box binding protein 1 (YB-1) is mediated by its cold shock domain and modulated by disordered terminal domains. *PLoS ONE* **7**, e36969.

Han, Y., Mu, Y., Li, X., Xu, P., Tong, J., Liu, Z., Ma, T., Zeng, G., Yang, S., Du, J. et al. (2011). Grhl2 deficiency impairs otic development and hearing ability in a zebrafish model of the progressive dominant hearing loss DFNA28. *Hum. Mol. Genet.* **20**, 3213-3226.

Hart, N. H. (1990). Fertilization in teleost fishes: mechanisms of sperm-egg interactions. *Int. Rev. Cytol.* **121**, 1-66.

Holm, P. S., Bergmann, S., Jürchott, K., Lage, H., Brand, K., Ladhoff, A., Mantwill, K., Curiel, D. T., Dobbelstein, M., Dietel, M. et al. (2002). YB-1 relocates to the nucleus in adenovirus-infected cells and facilitates viral replication by inducing E2 gene expression through the E2 late promoter. *J. Biol. Chem.* **277**, 10427-10434.

Kato, M., Han, T. W., Xie, S., Shi, K., Du, X., Wu, L. C., Mirzaei, H., Goldsmith, E. J., Longgood, J., Pei, J. et al. (2012). Cell-free formation of RNA granules: low complexity sequence domains form dynamic fibers within hydrogels. *Cell* **149**, 753-767.

Kaufman, R. J. (2002). Orchestrating the unfolded protein response in health and disease. *J. Clin. Invest.* **110**, 1389-1398.

Kimmel, C. B., Ballard, W. W., Kimmel, S. R., Ullmann, B. and Schilling, T. F. (1995). Stages of embryonic development of the zebrafish. *Dev. Dyn.* **203**, 253-310.

Kohno, K., Izumi, H., Uchiumi, T., Ashizuka, M. and Kuwano, M. (2003). The pleiotropic functions of the Y-box-binding protein, YB-1. *BioEssays* **25**, 691-698.
Kolluri, R., Torrey, T. A. and Kinniburgh, A. J. (1992). A CT promoter element binding protein: definition of a double-strand and a novel single-strand DNA binding motif. *Nucleic Acids Res.* **20**, 111-116.
Kumari, P., Gilligan, P. C., Lim, S., Tran, L. D., Winkler, S., Philp, R. and Sampath, K. (2013). An essential role for maternal control of Nodal signaling. *Elife* **2**, e00683.
Ladomery, M., Wade, E. and Sommerville, J. (1997). Xp54, the Xenopus homologue of human RNA helicase p54, is an integral component of stored mRNP particles in oocytes. *Nucleic Acids Res.* **25**, 965-973.
Lee, M. T., Bonneau, A. R., Takacs, C. M., Bazzini, A. A., DiVito, K. R., Fleming, E. S. and Giraldez, A. J. (2013). Nanog, Pou5f1 and SoxB1 activate zygotic gene expression during the maternal-to-zygotic transition. *Nature* **503**, 360-364.
Lee, M. T., Bonneau, A. R. and Giraldez, A. J. (2014). Zygotic genome activation during the maternal-to-zygotic transition. *Annu. Rev. Cell Dev. Biol.* **30**, 581-613.
Liu, X., Xiong, C., Jia, S., Zhang, Y., Chen, Y.-G., Wang, Q. and Meng, A. (2013). Araf kinase antagonizes Nodal-Smad2 activity in mesendoderm development by directly phosphorylating the Smad2 linker region. *Nat. Commun.* **4**, 1728.
Li-Villarreal, N., Forbes, M. M., Loza, A. J., Chen, J., Ma, T., Helde, K., Moens, C. B., Shin, J., Sawada, A., Hindes, A. E. et al. (2015). Dachsous1b cadherin regulates actin and microtubule cytoskeleton during early zebrafish embryogenesis. *Development* **142**, 2704-2718.
Lu, Z. H., Books, J. T. and Ley, T. J. (2005). YB-1 is important for late-stage embryonic development, optimal cellular stress responses, and the prevention of premature senescence. *Mol. Cell. Biol.* **25**, 4625-4637.
Lyons, S. M., Achorn, C., Kedersha, N. L., Anderson, P. J. and Ivanov, P. (2016). YB-1 regulates tiRNA-induced Stress Granule formation but not translational repression. *Nucleic Acids Res.* **44**, 6949-6960.
Medvedev, S., Pan, H. and Schultz, R. M. (2011). Absence of MSY2 in mouse oocytes perturbs oocyte growth and maturation, RNA stability, and the transcriptome. *Biol. Reprod.* **85**, 575-583.
Mendieta-Serrano, M. A., Schnabel, D., Lomelí, H. and Salas-Vidal, E. (2013). Cell proliferation patterns in early zebrafish development. *Anat. Rec. (Hoboken)* **296**, 759-773.
Meric, F., Matsumoto, K. and Wolffe, A. P. (1997). Regulated unmasking of in vivo synthesized maternal mRNA at oocyte maturation. A role for the chaperone nucleoplasmin. *J. Biol. Chem.* **272**, 12840-12846.
Miao, L., Yuan, Y., Cheng, F., Fang, J., Zhou, F., Ma, W., Jiang, Y., Huang, X., Wang, Y., Shan, L. et al. (2017). Translation repression by maternal RNA binding protein Zar1 is essential for early oogenesis in zebrafish. *Development* **144**, 128-138.
Minich, W. B., Maidebura, I. P. and Ovchinnikov, L. P. (1993). Purification and characterization of the major 50-kDa repressor protein from cytoplasmic mRNP of rabbit reticulocytes. *Eur. J. Biochem.* **212**, 633-638.
Montague, T. G., Cruz, J. M., Gagnon, J. A., Church, G. M. and Valen, E. (2014). CHOPCHOP: a CRISPR/Cas9 and TALEN web tool for genome editing. *Nucleic Acids Res.* **42**, W401-W407.
Murray, M. T., Schiller, D. L. and Franke, W. W. (1992). Sequence analysis of cytoplasmic mRNA-binding proteins of Xenopus oocytes identifies a family of RNA-binding proteins. *Proc. Natl. Acad. Sci. USA* **89**, 11-15.
Nair, S., Lindeman, R. E. and Pelegri, F. (2013). In vitro oocyte culture-based manipulation of zebrafish maternal genes. *Dev. Dyn.* **242**, 44-52.
Ohga, T., Uchiumi, T., Makino, Y., Koike, K., Wada, M., Kuwano, M. and Kohno, K. (1998). Direct involvement of the Y-box binding protein YB-1 in genotoxic stress-induced activation of the human multidrug resistance 1 gene. *J. Biol. Chem.* **273**, 5997-6000.
Pause, A., Belsham, G. J., Gingras, A.-C., Donzé, O., Lin, T.-A., Lawrence, J. C., Jr. and Sonenberg, N. (1994). Insulin-dependent stimulation of protein synthesis by phosphorylation of a regulator of 5′-cap function. *Nature* **371**, 762-767.
Rabani, M., Raychowdhury, R., Jovanovic, M., Rooney, M., Stumpo, D. J., Pauli, A., Hacohen, N., Schier, A. F., Blackshear, P. J., Friedman, N. et al. (2014). High-resolution sequencing and modeling identifies distinct dynamic RNA regulatory strategies. *Cell* **159**, 1698-1710.
Robertson, E. J. (2014). Dose-dependent Nodal/Smad signals pattern the early mouse embryo. *Semin. Cell Dev. Biol.* **32**, 73-79.
Schägger, H. (2006). Tricine-SDS-PAGE. *Nat. Protoc.* **1**, 16-22.
Schier, A. F. (2007). The maternal-zygotic transition: death and birth of RNAs. *Science* **316**, 406-407.
Schier, A. F. and Shen, M. M. (2000). Nodal signalling in vertebrate development. *Nature* **403**, 385-389.
Schmidt, E. K., Clavarino, G., Ceppi, M. and Pierre, P. (2009). SUnSET, a nonradioactive method to monitor protein synthesis. *Nat. Methods* **6**, 275-277.
Schröder, M. and Kaufman, R. J. (2005). The mammalian unfolded protein response. *Annu. Rev. Biochem.* **74**, 739-789.
Seki, S., Kouya, T., Tsuchiya, R., Valdez, D. M., Jr, Jin, B., Hara, T., Saida, N., Kasai, M. and Edashige, K. (2008). Development of a reliable in vitro maturation system for zebrafish oocytes. *Reproduction* **135**, 285-292.
Sha, Q.-Q., Dai, X.-X., Dang, Y., Tang, F., Liu, J., Zhang, Y.-L. and Fan, H.-Y. (2017). A MAPK cascade couples maternal mRNA translation and degradation to meiotic cell cycle progression in mouse oocytes. *Development* **144**, 452-463.
Shurtleff, M. J., Temoche-Diaz, M. M., Karfilis, K. V., Ri, S. and Schekman, R. (2016). Y-box protein 1 is required to sort microRNAs into exosomes in cells and in a cell-free reaction. *Elife* **5**, e19276.
Shurtleff, M. J., Yao, J., Qin, Y., Nottingham, R. M., Temoche-Diaz, M. M., Schekman, R. and Lambowitz, A. M. (2017). Broad role for YBX1 in defining the small noncoding RNA composition of exosomes. *Proc. Natl. Acad. Sci. USA* **114**, E8987-E8995.
Somasekharan, S. P., El-Naggar, A., Leprivier, G., Cheng, H., Hajee, S., Grunewald, T. G., Zhang, F., Ng, T., Delattre, O., Evdokimova, V. et al. (2015). YB-1 regulates stress granule formation and tumor progression by translationally activating G3BP1. *J. Cell Biol.* **208**, 913-929.
Sommerville, J. and Ladomery, M. (1996). Masking of mRNA by Y-box proteins. *FASEB J.* **10**, 435-443.
Subtelny, A. O., Eichhorn, S. W., Chen, G. R., Sive, H. and Bartel, D. P. (2014). Poly(A)-tail profiling reveals an embryonic switch in translational control. *Nature* **508**, 66-71.
Svitkin, Y. V., Evdokimova, V. M., Brasey, A., Pestova, T. V., Fantus, D., Yanagiya, A., Imataka, H., Skabkin, M. A., Ovchinnikov, L. P., Merrick, W. C. et al. (2009). General RNA-binding proteins have a function in poly(A)-binding protein-dependent translation. *EMBO J.* **28**, 58-68.
Tadros, W. and Lipshitz, H. D. (2009). The maternal-to-zygotic transition: a play in two acts. *Development* **136**, 3033-3042.
Tadros, W., Goldman, A. L., Babak, T., Menzies, F., Vardy, L., Orr-Weaver, T., Hughes, T. R., Westwood, J. T., Smibert, C. A. and Lipshitz, H. D. (2007). SMAUG is a major regulator of maternal mRNA destabilization in Drosophila and its translation is activated by the PAN GU kinase. *Dev. Cell* **12**, 143-155.
Tafuri, S. R. and Wolffe, A. P. (1993). Selective recruitment of masked maternal mRNA from messenger ribonucleoprotein particles containing FRGY2 (mRNP4). *J. Biol. Chem.* **268**, 24255-24261.
Tafuri, S. R., Familari, M. and Wolffe, A. P. (1993). A mouse Y box protein, MSY1, is associated with paternal mRNA in spermatocytes. *J. Biol. Chem.* **268**, 12213-12220.
Tokumoto, T., Yamaguchi, T., Ii, S. and Tokumoto, M. (2011). In vivo induction of oocyte maturation and ovulation in zebrafish. *PLoS ONE* **6**, e25206.
Trapnell, C., Pachter, L. and Salzberg, S. L. (2009). TopHat: discovering splice junctions with RNA-Seq. *Bioinformatics* **25**, 1105-1111.
Uchiumi, T., Fotovati, A., Sasaguri, T., Shibahara, K., Shimada, T., Fukuda, T., Nakamura, T., Izumi, H., Tsuzuki, T., Kuwano, M. et al. (2006). YB-1 is important for an early stage embryonic development: neural tube formation and cell proliferation. *J. Biol. Chem.* **281**, 40440-40449.
Winata, C. L., Lapinski, M., Pryszcz, L., Vaz, C., Bin Ismail, M. H., Nama, S., Hajan, H. S., Lee, S. G. P., Korzh, V., Sampath, P. et al. (2018). Cytoplasmic polyadenylation-mediated translational control of maternal mRNAs directs maternal-to-zygotic transition. *Development* **145**, dev159566.
Wolffe, A. P. (1994). Structural and functional properties of the evolutionarily ancient Y-box family of nucleic acid binding proteins. *BioEssays* **16**, 245-251.
Wolffe, A. P., Tafuri, S., Ranjan, M. and Familari, M. (1992). The Y-box factors: a family of nucleic acid binding proteins conserved from Escherichia coli to man. *New Biol.* **4**, 290-298.
Wu, B., Chao, J. A. and Singer, R. H. (2012). Fluorescence fluctuation spectroscopy enables quantitative imaging of single mRNAs in living cells. *Biophys. J.* **102**, 2936-2944.
Wu, S.-L., Fu, X., Huang, J., Jia, T.-T., Zong, F.-Y., Mu, S.-R., Zhu, H., Yan, Y., Qiu, S., Wu, Q. et al. (2015). Genome-wide analysis of YB-1-RNA interactions reveals a novel role of YB-1 in miRNA processing in glioblastoma multiforme. *Nucleic Acids Res.* **43**, 8516-8528.
Xu, P., Zhu, G., Wang, Y., Sun, J., Liu, X., Chen, Y.-G. and Meng, A. (2014). Maternal Eomesodermin regulates zygotic nodal gene expression for mesendoderm induction in zebrafish embryos. *J. Mol. Cell Biol.* **6**, 272-285.
Yang, W.-H. and Bloch, D. B. (2007). Probing the mRNA processing body using protein macroarrays and “autoantigenomics”. *RNA* **13**, 704-712.
Yang, J., Medvedev, S., Yu, J., Tang, L. C., Agno, J. E., Matzuk, M. M., Schultz, R. M. and Hecht, N. B. (2005). Absence of the DNA-/RNA-binding protein MSY2 results in male and female infertility. *Proc. Natl. Acad. Sci. USA* **102**, 5755-5760.
Yang, J., Morales, C. R., Medvedev, S., Schultz, R. M. and Hecht, N. B. (2007). In the absence of the mouse DNA/RNA-binding protein MSY2, messenger RNA instability leads to spermatogenic arrest. *Biol. Reprod.* **76**, 48-54.
Yao, L., Chen, J., Wu, X., Jia, S. and Meng, A. (2017). Zebrafish cdc6 hypomorphic mutation causes Meier-Gorlin syndrome-like phenotype. *Hum. Mol. Genet.* **26**, 4168-4180.
Yartseva, V. and Giraldez, A. J. (2015). The maternal-to-zygotic transition during vertebrate development: a model for reprogramming. *Curr. Top. Dev. Biol.* **113**, 191-232.
Yoshida, H., Matsui, T., Yamamoto, A., Okada, T. and Mori, K. (2001). XBP1 mRNA is induced by ATF6 and spliced by IRE1 in response to ER stress to produce a highly active transcription factor. *Cell* **107**, 881-891.

Development (2018) 145, dev166587. doi:10.1242/dev.166587

Yu, J., Hecht, N. B. and Schultz, R. M. (2002). RNA-binding properties and translation repression in vitro by germ cell-specific MSY2 protein. *Biol. Reprod.* **67**, 1093-1098.

Zaucker, A., Nagorska, A., Kumari, P., Hecker, N., Wang, Y., Huang, S., Cooper, L., Sivashanmugam, L., VijayKumar, S., Brosens, J. et al. (2018). Translational co-regulation of a ligand and inhibitor by a conserved RNA element. *Nucleic Acids Res.* **46**, 104-119.

Zhao, B. S., Wang, X., Beadell, A. V., Lu, Z., Shi, H., Kuuspalu, A., Ho, R. K. and He, C. (2017). m(6)A-dependent maternal mRNA clearance facilitates zebrafish maternal-to-zygotic transition. *Nature* **542**, 475-478.

Supplementary figures

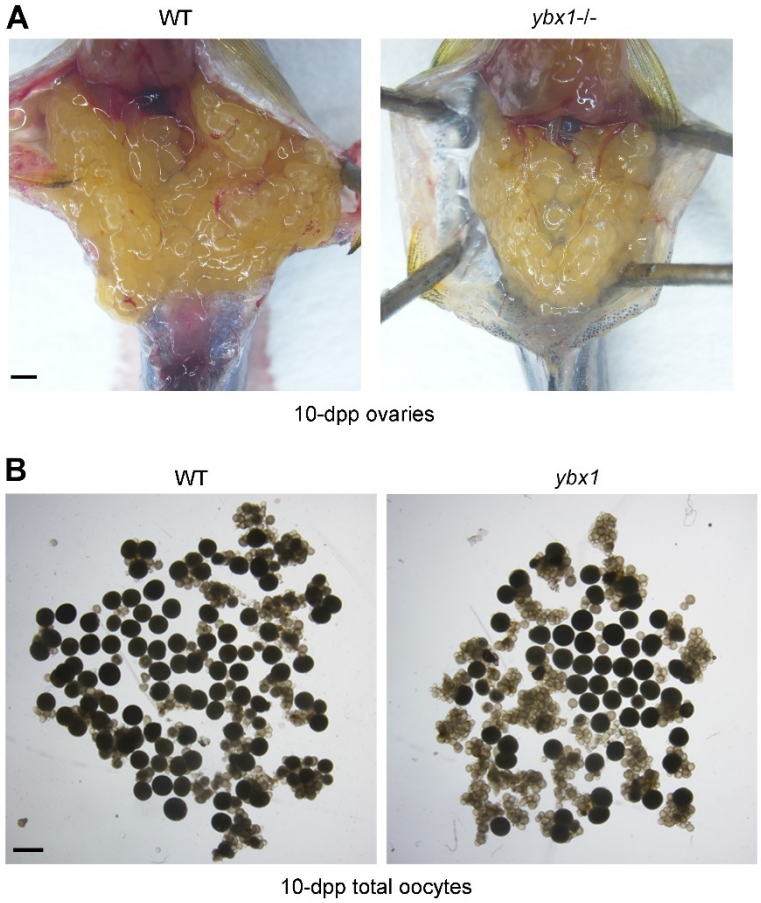

Fig. S1. Ovaries and oocytes from WT and *Zybx1* females. (A) Ovaries from WT and *Zybx1* females at 10 dpp. Mature eggs were purged from female fish via natural matings on Day 1. On Day 11 (10 dpp), female fish were sacrificed. (B) Total oocytes from WT and *Zybx1* female fish at 10 dpp. Scale bars: 1 mm.

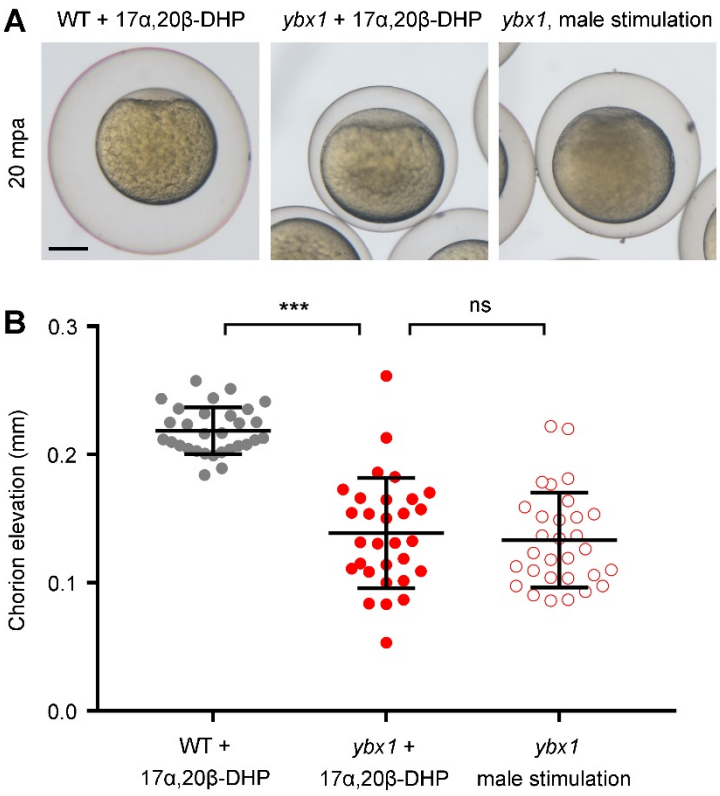

Fig. S2. Hormonal stimulation cannot rescue the egg activation defect caused by Ybx1 depletion. (A) Representative images of activated eggs with chorions. Eggs from 17α,20β-DHP-treated WT female fish, 17α,20β-DHP-treated Z*ybx1* female fish and male fish-stimulated Z*ybx1* female fish are shown from left to right. mpa, minutes post-activation. Chorion expansion after water activation was used as the criterion for evaluating oocyte maturation and egg activation. (B) Measurement of chorion elevation distances at 20 mpa. ns, not significant; ***P<0.001; Welch's t-test.

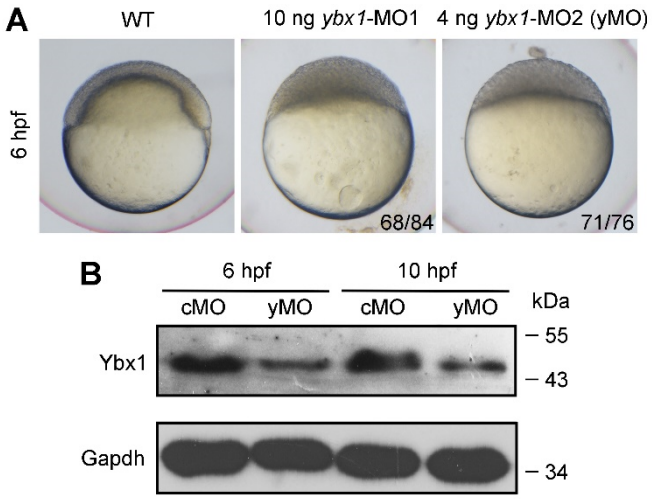

Fig. S3. Knockdown of *ybx1* expression by translation-blocking morpholinos. (A) Bright-field images of a WT embryo and embryos injected with 10 ng *ybx1*-MO1 or 4 ng *ybx1*-MO2. 4 ng *ybx1*-MO2 was injected in subsequently described experiments as yMO. (B) Examination of yMO-mediated *ybx1* knockdown efficiency. Endogenous Ybx1 and Gapdh were detected by western blotting.

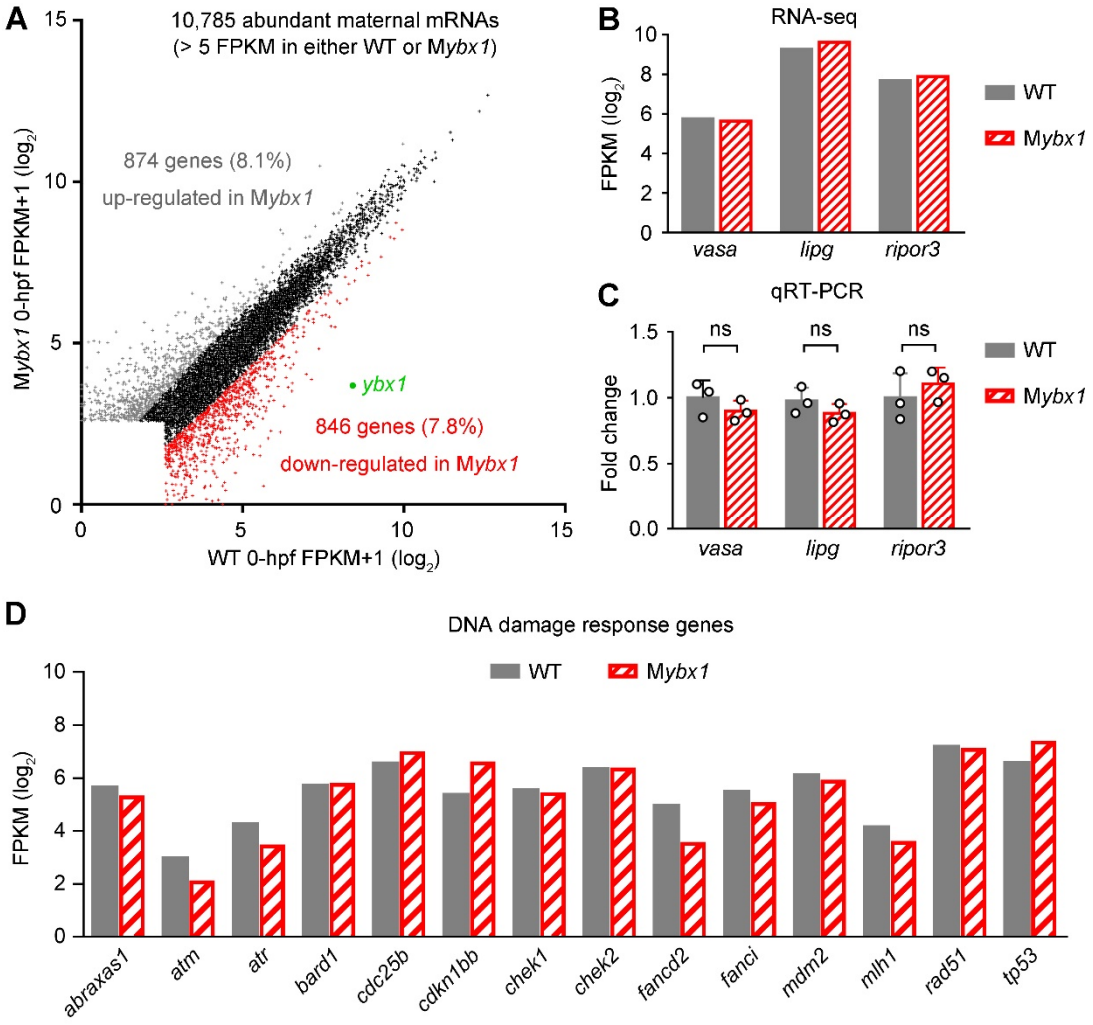

Fig. S4. Maternal transcriptome analysis of WT and M*ybx1* embryos. (A) Plotting of individual gene expression levels (FPKM+1, $\log_2$) in 0-hpf WT and M*ybx1* embryos. 10,785 genes with abundant maternal mRNA deposition (>5 FPKM in either WT or M*ybx1* embryo at 0 hpf) were plotted. Genes with >2-fold FPKM increases and >50% decreases in M*ybx1* were considered up and down-regulated genes, respectively. (B,C) Approximately equal expression levels of *vasa*, *lipg* and *ripor3* in WT and M*ybx1* embryos determined by RNA-seq and qRT-PCR data. *GFP* mRNA was injected at one-cell stage embryos and was used as the reference for qPCR. ns, not significant; n=3; Student's *t*-test. (D) Expression levels of DNA damage response genes in 0-hpf WT and M*ybx1* embryos.

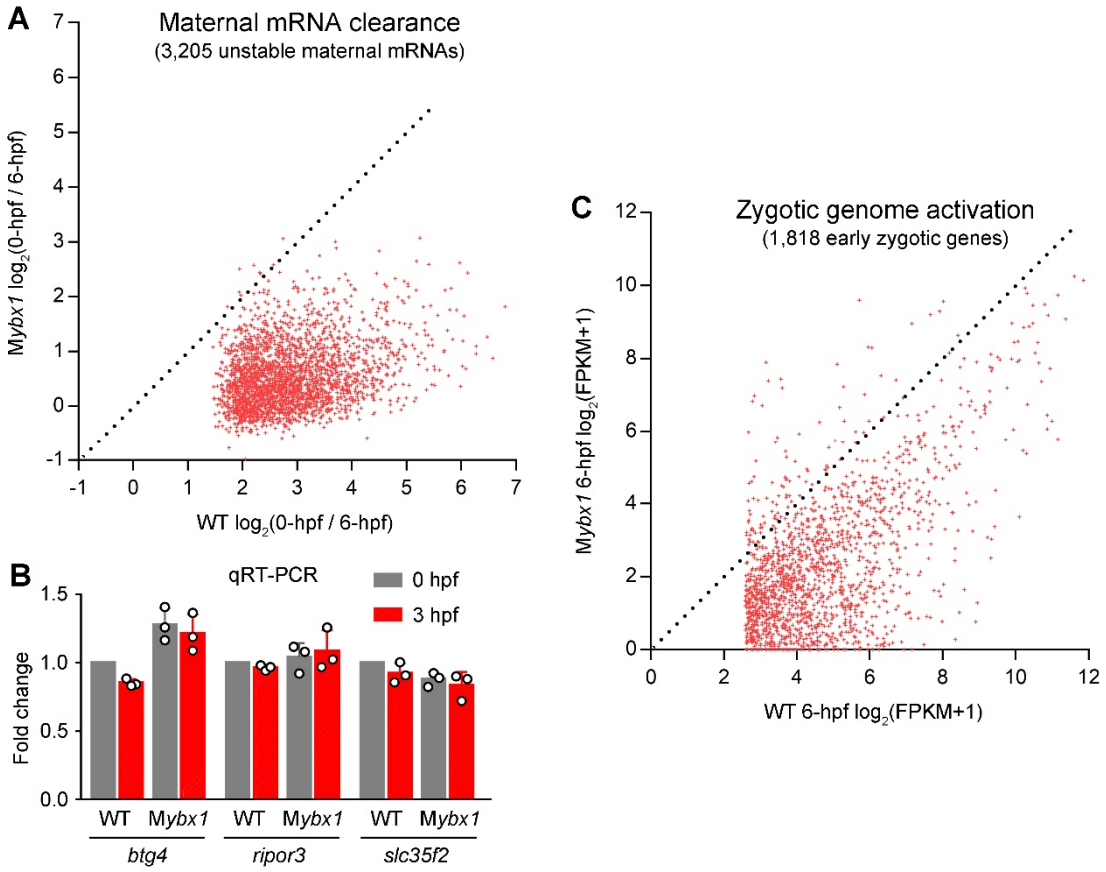

Fig. S5. Transcriptome analysis of the MZT process in M*ybx1* mutants. (A) Plotting of individual maternal mRNA degradation levels (0-hpf/6-hpf, log_2-scale) in WT and M*ybx1* embryos. 3,205 unstable maternal mRNAs were plotted. (B) qRT-PCR analysis of *btg4*, *ripor3* and *slc35f2* mRNA levels in 0-hpf and 3-hpf embryos. (C) Plotting of individual zygotic gene expression levels (log_2-scale) in 6-hpf WT and M*ybx1* embryos. 1,818 early zygotic genes were plotted. Dotted lines: y=x. (FPKM+1) values were calculated to include genes with 0 FPKM.

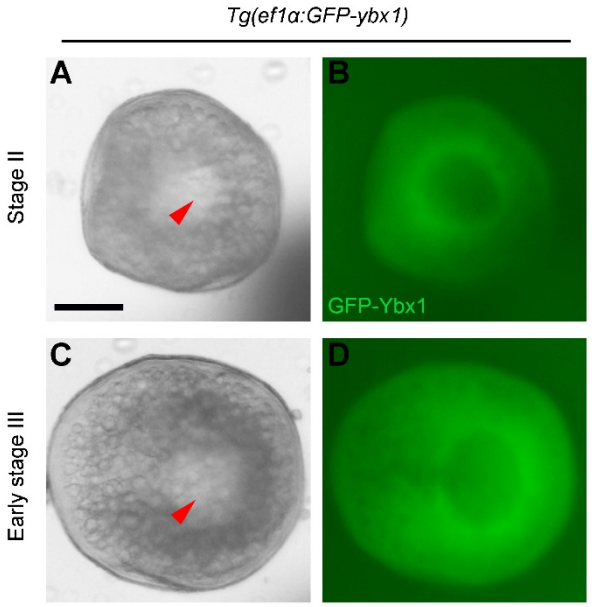

Fig. S6. GFP-Ybx1 expression in oocytes. Expression of GFP-Ybx1 fusion protein in *Tg(ef1α:GFP-ybx1)* oocytes at stage II (A,B) and early stage III (C,D). (A,B) Bright-field images. (C,D) Fluorescent images. Red arrowheads indicate oocyte nuclei. Scale bar: 100 µm.

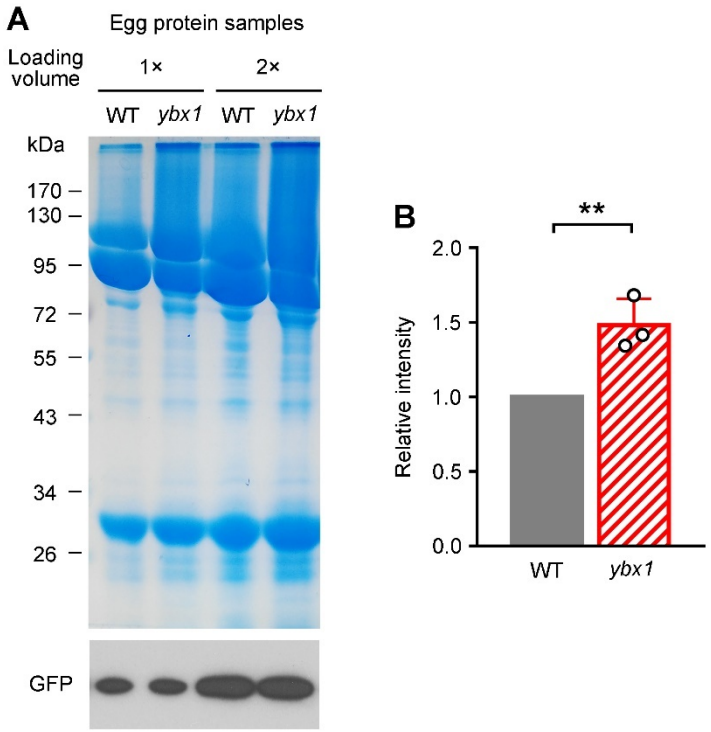

Fig. S7. Increase of global protein level in *ybx1* mutant eggs. (A) SDS-PAGE and Coomassie staining showing global protein levels in WT and *ybx1* mutant eggs. GFP protein was injected into eggs as the loading control. (B) Relative lane intensities quantified in the Coomassie staining images. Western blotting signal of GFP served as the control. ***P*<0.01; n=3; Student's *t*-test.

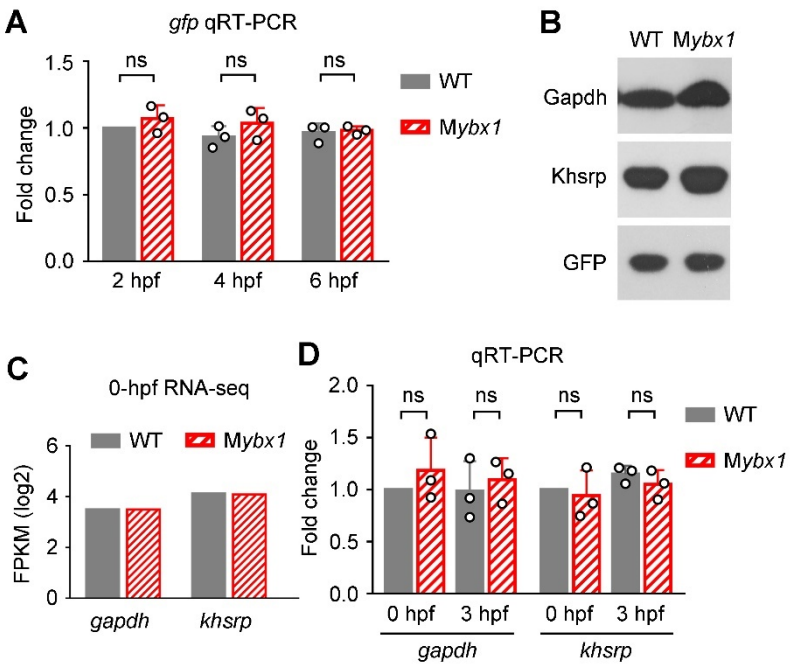

Fig. S8. Analysis of mRNA stability in WT and M*ybx1* embryos. (A) qRT-PCR analysis of injected *gfp* mRNA levels in 2-hpf, 4-hpf and 6-hpf embryos. (B) Western blotting analysis of Gapdh and Khsrp protein levels in 3-hpf WT and M*ybx1* embryos. Injected GFP protein was used as the loading control. (C) Gene expression levels of *gapdh* and *khsrp* in 0-hpf RNA-seq data. (D) qRT-PCR analysis of *gapdh* and *khsrp* mRNA levels in 0-hpf and 3-hpf embryos. ns, not significant; n=3; Student's *t*-test.

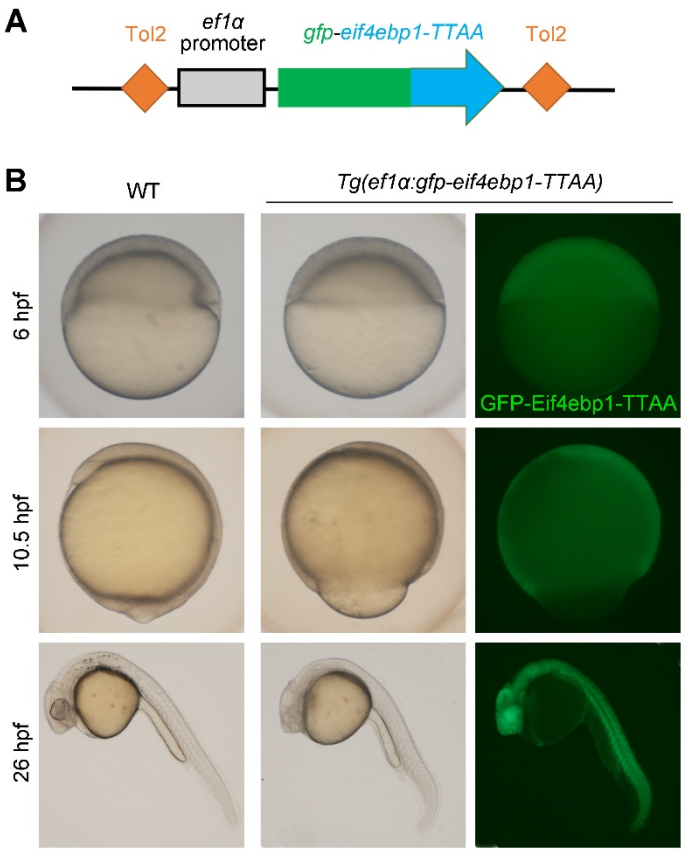

Fig. S9. The transgenic zebrafish line expressing a CA form of Eif4ebp1. (A) A diagram of the zebrafish *ef1α* promoter-driven *gfp-eif4ebp1-TTAA* transgene. (B) Bright-field and fluorescent images of *Tg(ef1α:gfp-eif4ebp1-TTAA)* embryos at 6 hpf, 10.5 hpf and 26 hpf, showing expression of Eif4ebp1-TTAA and the resulted developmental delay.

Supplementary tables

Table S1. PCR primers for *ybx1* mutant genotyping.

Primer	Sequence
ybx1-target-F	CTCAGTCCGTCCAGTTCGAT
ybx1-target-R	AAAATACCAGGCAGGACGCC
ybx1-wt-F	CAGCTACCGCGGGGGATAA
ybx1-mut-F	CGCAGCTACCGCGGTCATC

Table S2. qRT-PCR and RT-PCR primers.

Primer	Sequence
ybx1-F	TTCGACGTGGTAGAAGGGGA
ybx1-R	ACCTTCACCACCCTCTGTCA
vasa-F	CCAGAGTCTGACACTCCATTAGCTC
vasa-R	GAGCACTGAAGGCAACTTCCTC
gfp-F	GTGGTGCCCATCCTGGTC
gfp-R	CCGGTGGTGCAGATGAACTT
btg4-F	TGTCATGCCGGTATGGTGAA
btg4-R	GTTGGGATGCATTTGGGCTC
casd1-F	GCATTCTGGAATCTGGCCCT
casd1-R	TGACCACAGCAAATCGGTCC
cldnd-F	ACAATGGCATCTGTTGGGCT
cldnd-R	GTTCATCCAGAGGCCTTCCC
lipg-F	CACTTGGGGTCCTCGTTCTT
lipg-R	GTAGTGCAATCGTTTCCTGGG
ripor3-F	TGAGGAAGGGACTCAAGGACT
ripor3-R	ACAGCCGCCACTGAATACAA
slc35f2-F	TGGGGTGCAAATGGCTATACT

slc35f2-R	TTACCACCACAGGCACGAAA
acadl-F	CCACATCAGCAGCATGTTCG
acadl-R	CGTTTTGCCTGAACAGGTCG
cd82b-F	CAGCTGCTCCACGGATCTTC
cd82b-R	ATGCAACCCAGGAATCCCAT
apoeb-F	CACACAAACTGACGGCATGG
apoeb-R	GCATATGGGGTCATCTGGG
cxcr4b-F	GCGCCTTTTTGAGCACACTT
cxcr4b-R	ATTGCTGACTGAGAGGTCGC
dusp6-F	TTGCAGGCATCAGTCGTTCT
dusp6-R	TCCTAACGTGCGCTCAAAGT
fgfr4-F	CAGAGCGACGTATGGTCTTT
fgfr4-R	AGGTGTCCTCACAAGATGGA
grhl3-F	ATGGAGAGGACGGCAAACAG
grhl3-R	AGGTGTGGCCTCCAGAAAG
nnr-F	CGCAGAGATGGACAGCGATT
nnr-R	ATATTGGCCTCGTCTGGAGC
vent-F	AAACTCAGGTGAAGACGTGG
vent-R	AGAAGTAGCAGCGTGTGAAC
wnt11-F	CACACAGAACGCCAAACAGG
wnt11-R	CAGACGTATCTCTCGACGG
gapdh-F	ACAGCAACACAGAAGACCGT
gapdh-R	GGCAGGTTTCTCAAGACGGA
khsrp-F	AGAGTGTTCGTCCTTCGTCG
khsrp-R	CCACTGTCTGGAGCGATCTG
xbp1-slicing-F	AGGAGATCAGACTCAGAGTCTG
xbp1-splicing-R	GAGACAAGACGAGTGATCTGCT
actb2-F	ATGGATGATGAAATTGCCGCAC

actb2-R	ACCATCACCAGAGTCCATCACG
atf3-F	ATCACAAACACACGCGCCTA
atf3-R	TTTGTGAAGTCGTCCAGCGT

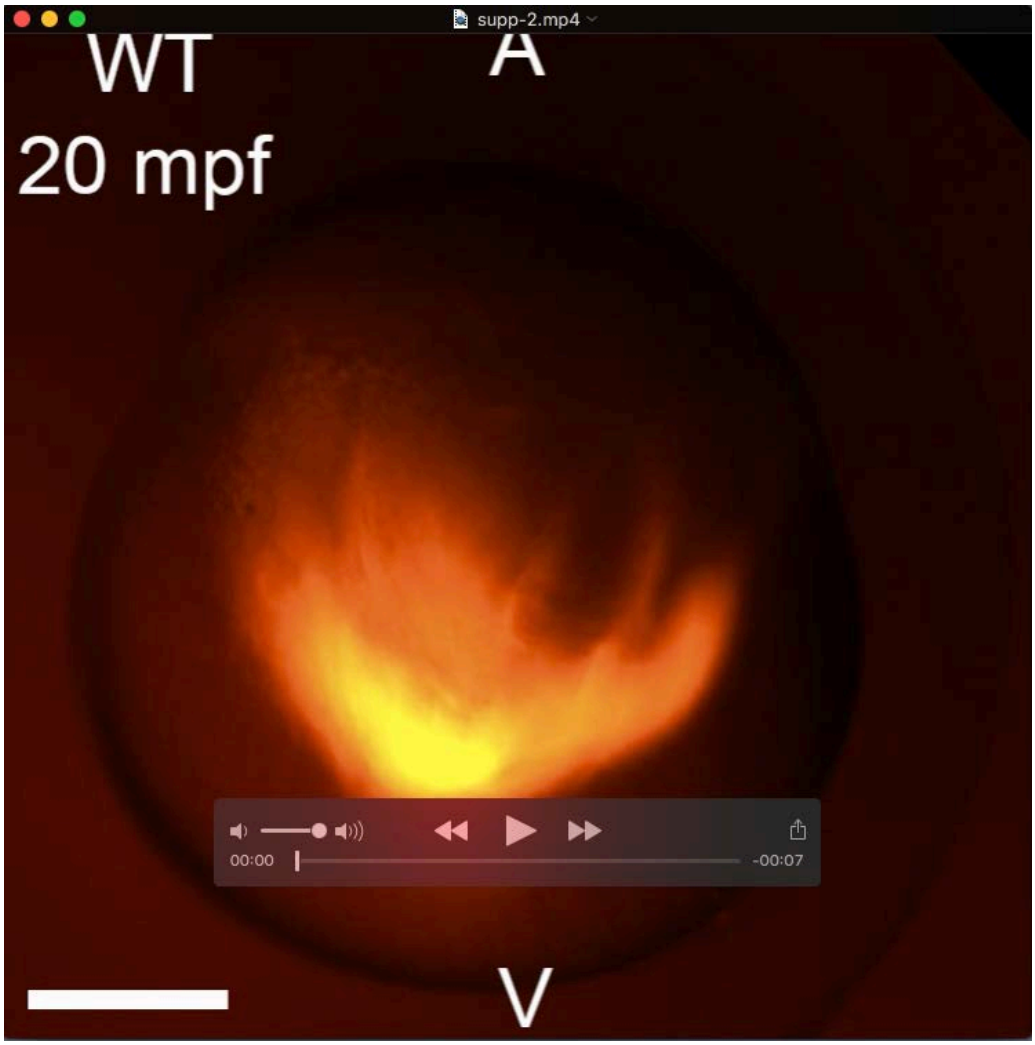

Movie 1. Cytoplasmic movement in a WT embryo from 20 mpf to 40 mpf. Rhodamine dye was injected at 10 mpf and embryos were imaged from 20 mpf to 40 mpf. The persistent cytoplasmic streaming that transports rhodamine to the animal pole can be visualized. 8 embryos were observed and this movie shows the representative result. A, animal pole; V, vegetal pole. Scale bar: 200 μm.

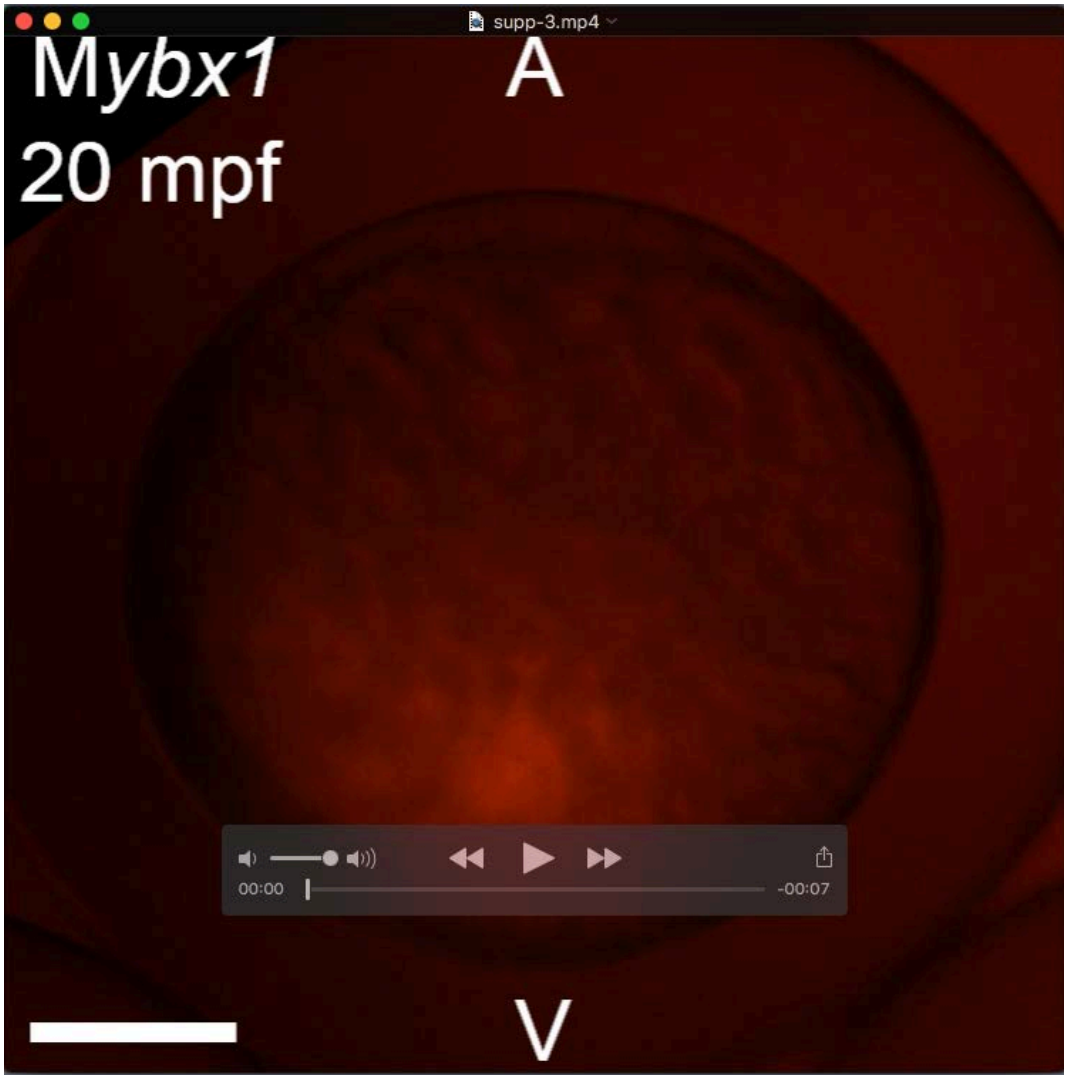

Movie 2. Cytoplasmic movement in an M*ybx1* embryo from 20 mpf to 40 mpf. Rhodamine dye was injected at 10 mpf and embryos were imaged from 20 mpf to 40 mpf. Due to the opaqueness of M*ybx1* embryos, the rhodamine fluorescence is relatively weak and scattered. The cytoplasmic movement is stagnant and the transportation of rhodamine is highly inefficient. 5 embryos were observed and this movie shows the representative result. A, animal pole; V, vegetal pole. Scale bar: 200 μm.

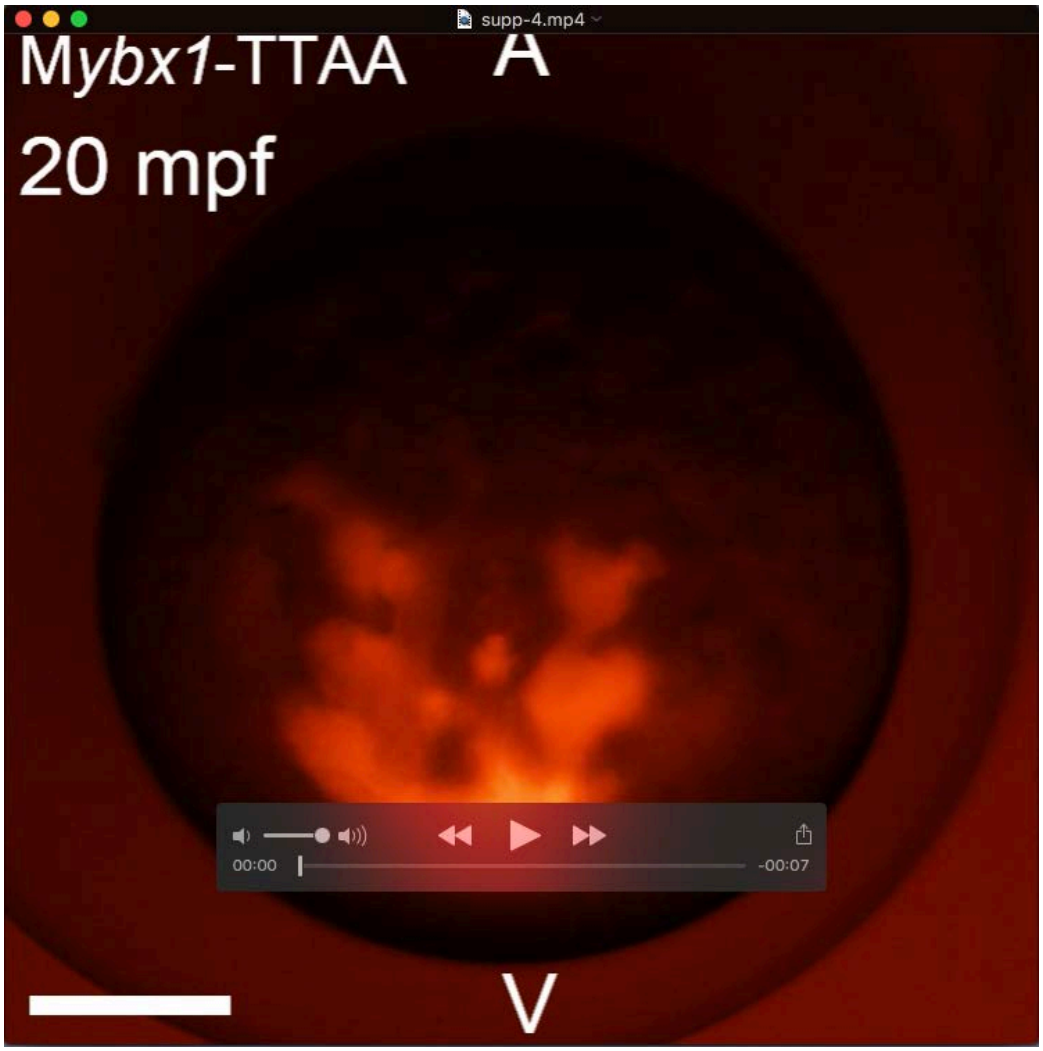

Movie 3. Cytoplasmic movement in an M*ybx1*-TTAA embryo from 20 mpf to 40 mpf. Rhodamine dye was injected at 10 mpf and embryos were imaged from 20 mpf to 40 mpf. Compared to M*ybx1* embryos (Movie 2), the cytoplasmic movement is partially restored. 6 embryos were observed and this movie shows the representative result. A, animal pole; V, vegetal pole. Scale bar: 200 μm.